New flavonoid – *N,N*-dibenzyl(*N*-methyl)amine hybrids: Multi-target-directed agents for Alzheimer´s disease endowed with neurogenic properties

Martín Estrada-Valencia, Clara Herrera-Arozamena, Concepción Pérez, Dolores Viña, José A. Morales-García, Ana Pérez-Castillo, Eva Ramos, Alejandro Romero, Erik Laurini, Sabrina Pricl & María Isabel Rodríguez-Franco

View supplementary material

Published online: 07 Mar 2019.

Submit your article to this journal
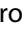
View Crossmark data

Taylor & Francis
Taylor & Francis Group

RESEARCH PAPER

OPEN ACCESS Check for updates

New flavonoid – *N,N*-dibenzyl(*N*-methyl)amine hybrids: Multi-target-directed agents for Alzheimer's disease endowed with neurogenic properties

Martín Estrada-Valencia[a] (iD), Clara Herrera-Arozamena[a] (iD), Concepción Pérez[a] (iD), Dolores Viña[b] (iD), José A. Morales-García[c,d,e] (iD), Ana Pérez-Castillo[c,d] (iD), Eva Ramos[f] (iD), Alejandro Romero[f] (iD), Erik Laurini[g] (iD), Sabrina Pricl[g] (iD) and María Isabel Rodríguez-Franco[a] (iD)

[a]Institute of Medicinal Chemistry, Spanish Council for Scientific Research (IQM-CSIC), Madrid, Spain; [b]Centre for Research in Molecular Medicine and Chronic Diseases (CIMUS), University of Santiago de Compostela, Santiago de Compostela, Spain; [c]Institute for Biomedical Research "Alberto Sols", Spanish Council for Scientific Research (IIB-CSIC), Madrid, Spain; [d]Biomedical Research Networking Centre on Neurodegenerative Diseases (CIBERNED), Madrid, Spain; [e]Department of Cellular Biology, Medical School, Complutense University of Madrid, Madrid, Spain; [f]Department of Pharmacology and Toxicology, Faculty of Veterinary Medicine, Complutense University of Madrid, Madrid, Spain; x[g]Molecular Biology and Nanotechnology Laboratory (MolBNL@UniTS), Department of Engineering and Architecture (DEA), Trieste, Italy

ABSTRACT

The design of multi-target directed ligands (MTDLs) is a valid approach for obtaining effective drugs for complex pathologies. MTDLs that combine neuro-repair properties and block the first steps of neurotoxic cascades could be the so long wanted remedies to treat neurodegenerative diseases (NDs). By linking two privileged scaffolds with well-known activities in ND-targets, the flavonoid and the *N,N*-dibenzyl(*N*-methyl)-amine (DBMA) fragments, new CNS-permeable flavonoid – DBMA hybrids (**1–13**) were obtained. They were subjected to biological evaluation in a battery of targets involved in Alzheimer's disease (AD) and other NDs, namely human cholinesterases (hAChE/hBuChE), β-secretase (hBACE-1), monoamine oxidases (hMAO-A/B), lipoxygenase-5 (hLOX-5) and sigma receptors (σ_1R/σ_2R). After a funnel-type screening, 6,7-dimethoxychromone – DBMA (**6**) was highlighted due to its neurogenic properties and an interesting MTD-profile in hAChE, hLOX-5, hBACE-1 and σ_1R. Molecular dynamic simulations showed the most relevant drug-protein interactions of hybrid **6**, which could synergistically contribute to neuronal regeneration and block neurodegeneration.

Introduction

Despite the great advances achieved in the understanding of the Alzheimer's disease (AD) pathophysiology, our current knowledge about this illness is still an incomplete puzzle. Based on different causative factors, several hypotheses have tried to explain its origin, such as the amyloid-beta peptide (Aβ) accumulation, abnormal *tau* phosphorylation, cholinergic transmission deficits, exacerbated neuroinflammatory response and oxidative damage. Nevertheless, up to date, all of them are just loose pieces of the puzzle, and none of them is able to account for the complexity of AD[1].

This brings us to the main fact that is clear today, the multifactorial nature of this disease, in which different factors contribute to its onset and progression. However, the current approved drugs are mainly active at a single target, acetylcholinesterase (AChE) or *N*-methyl-D-aspartate receptor (NMDA), that have barely been able to modify the disease progression[2]. This failure lies in the complex network of pathophysiological processes underlying the origin of the AD-related neurodegeneration, and in our lack of knowledge about the primordial event that triggers the others, if there is only one. So far, we understand that genetic, epigenetic and environmental factors are involved in neurodegeneration.

Moreover, increasing evidence suggests that some systemic alterations in AD should be understood as the echo of underlying processes related to the origin of the disease and not only as secondary effects of neuronal death. Some of these systemic alterations include abnormalities in immunity and antioxidant responses, metabolic disorders, hepatic dysfunction, cardiovascular diseases and gut microbiota disturbance, among others[3]. This reveals that a multifactorial process such as AD cannot be stopped or prevented with a treatment based on a single and simple mechanism of action.

From these ideas, more holistic strategies must be explored, not only regarding to the pharmacological approach but to the whole body of research that is developing around the world related to neurodegeneration. From a pharmacological point of view, the multi-target directed ligand (MTDL) strategy has emerged as an alternative against the traditional single target – single molecule approach[4,5]. Indeed, in the last decade an increasing number of new drugs based on this paradigm have been developed for the treatment of several complex diseases. In the field of NDs, safinamide was approved in Europe in February 2015 and in the United States in March 2017 for the treatment of Parkinson's disease (PD), due to its MTD-profile that combines

dopaminergic (MAO-B and dopamine reuptake inhibition) and non-dopaminergic properties (blockade of voltage-dependent Na^+ and Ca^{2+} channels)[6]. Interestingly, to achieve maximum efficiency in stopping or delaying neurodegeneration, the MTD drugs must hit targets located upstream in the neurotoxic cascades[7,8].

Different post-mortem studies in AD patients have shown a great increase in the peroxidation of brain biomolecules[9], suggesting that oxidative damage is an early event that precedes the formation of abnormal protein aggregates and that antioxidant drugs could be useful for preventing such injuries[10]. On other hand, levels of monoamine oxidases (MAO-A and MAO-B) are increased in neurodegenerative pathologies, such as AD and PD[11]. The activities of these enzymes contribute to the neurodegenerative process by promoting the formation of the harmful Aβ peptide and by increasing the oxidative stress (OS) through the production of hydrogen peroxide[12]. Consequently, MAOs' inhibitors could decrease both the generation of amyloid plaques and radical oxygen/nitrogen species (ROS/RNS)[13].

Sequential cleavage of the amyloid precursor protein by β- and γ-secretases produces pathologic Aβ peptides, which are prone to aggregate into amyloid plaques[14]. The fact that β-secretase, also known as β-site amyloid-precursor-protein-cleaving enzyme 1 (BACE-1), is located upstream in the amyloid cascade makes its inhibitors interesting AD disease-modifying drugs[15]. In recent years, BACE-1 has gained great importance because several clinical trials have shown a correlation between the inhibition of this enzyme and low levels of pathological Aβ peptides[16,17]. In spite of the above, several potent BACE-1 inhibitors have failed in different clinical trials. For instance, verubecestat (MK-8931) a potent BACE-1 inhibitor, able to reduce Aβ levels in cerebrospinal fluid up to 81%, was ineffective in AD patients ranging from 55 to 85 years in phase III studies[18]. Although these negative results may lead us to reconsider the validity of the amyloid hypothesis, the results of current clinical trials of BACE-1 inhibitors in asymptomatic individuals at risk to develop AD or with prodromal AD are still to be seen[19]. From another point of view, issues associated to BACE-1 inhibitors could be related to the fact that they are administered to AD patients in the severe stages where they cannot provide any therapeutic benefit, or to the fact that these drugs are still based on the single-target paradigm. The situation is so complex that the ideal drug for AD should be administered in the right moment and has to be able to reduce neuronal death coming from almost all sources of toxicity: oxidative stress, misfolded proteins, excitotoxicity and so on. Therefore, we still consider important the search for new BACE-1 inhibitors, but endowed with a MTD-profile in light of the current literature[20].

Lipoxygenase-5 (LOX-5) is an enzyme widely distributed in central nervous system (CNS), mainly in neurons and glia. Two especially vulnerable regions to neurodegeneration, the cerebral cortex and the hippocampus, possess the highest expression levels of this enzyme that is upregulated in AD patients[21]. LOX-5 plays a key role in inflammatory processes, which *per se* may be an important reason for its pharmacological modulation, and interestingly, overexpression of LOX-5 in the AD-triple transgenic mouse model (3xTg) leads to a clear exacerbation of memory deficits and increased burdens of both *tau* and amyloid deposits[22]. Conversely, 3xTg mice treated with the LOX-5 inhibitor zileuton present an improvement in memory, cognition, synaptic integrity and a reduction in amyloid and *tau* pathologies[23]. These findings establish a functional role of LOX-5 in the AD-pathogenesis, pointing out the interest of LOX-5 inhibitors as valuable therapeutic agents, as they reduce neuro-inflammation and the main AD-hallmarks, amyloid plaques and neurofibrillary tangles.

On the other hand, the sigma-1 receptor (σ_1R) is a chaperone-like receptor located at the mitochondria-associated endoplasmic reticulum membrane, widely distributed in CNS and implicated in memory, emotional and cognitive processes. While the complete biological role of this receptor remains unknown, it has been discovered to regulate the function of a variety of processes through opioid, NMDA, dopaminergic and cholinergic receptors. Pharmacological or genetic invalidation of σ_1R enhances Aβ toxicity[24], whereas its activation exerts protection against OS by stimulation of the antioxidant response elements and subsequent transcription of the proteins involved in the cellular response to oxidative damage[25].

Although the adult neurogenic processes are restricted to specific small brain regions and a large characterisation of their extent and relevance is still needed[26,27], the pharmacological induction of neurogenesis is achievable and may significate a great opportunity to help the brain to recover its own self-renewal capacity[28,29]. Maybe the so desired disease-modifying AD-drug would include the ability to induce the differentiation of neural stem cells into mature neurons capable to replace those lost by neurodegeneration. In this regard, a promising compound is the steroid allopregnanolone that has demonstrated to promote neurogenic processes and reverse cognitive deficits in a mouse model of AD[30] and that recently completed phase-I studies[31].

In the last years, a part of our work has been focussed on the design of new compounds with a MTD-profile aiming at some of the most important pharmacological objectives related to AD and NDs. Apart from the classical targets (AChE, BACE-1, MAOs), other important proteins involved in NDs have been explored, such as σ_1R, LOX-5 and the activation of neurogenic processes[32–37]. Continuing with our interest in MTDLs, in this work we describe the synthesis of new flavonoid-based hybrids (**1–13**) and their biological evaluation in a battery of ND-targets, namely hAChE, hBACE-1, hMAOs, hLOX-5 and σ_1R, and in a phenotypic assay for assessing neurogenic properties.

New hybrids were designed by linking two privileged chemotypes with well-known therapeutic activities in AD and other NDs: (i) a flavonoid core derived from 4-chromenone or 4-quinolone, with potential neurogenic properties[38] and inhibition of BACE-1[39], LOX-5[40] and MAO[41]; and (ii) the *N,N*-dibenzyl(*N*-methyl)amine (DBMA) fragment, present in AP2238[42–44] and other AD-directed MTDLs[45,46], due to its proved interaction with the catalytic anionic site (CAS) of AChE[47] (Figure 1).

Materials and methods

Chemistry

Reagents and solvents were purchased from common commercial suppliers, mostly Sigma-Aldrich, and were used without further purification. Thin-layer chromatography (TLC) was carried out using Merck silica gel 60 F254 plates and compounds were visualised under UV-light ($\lambda = 254$ or 365 nm) and/or stained with phosphomolybdic acid 10% wt. in ethanol. Automatised chromatographic separation was carried out in an IsoleraOne (Biotage) equip, using different silica Biotage ZIP KP-Sil 50μ cartridges. High-performance liquid chromatography was performed on a Waters analytical HPLC-MS (Alliance Watters 2690) equipped with a SunFire C_{18} 4.6×50 mm column, a UV photodiode array detector ($\lambda = 214$–274 nm) and quadrupole mass spectrometer (Micromass ZQ). HPLC analyses were used to confirm the purity of all compounds ($\geq$ 95%) and were performed on Waters 6000 equipment, at a flow rate of 1.0 ml/min, with a UV photodiode
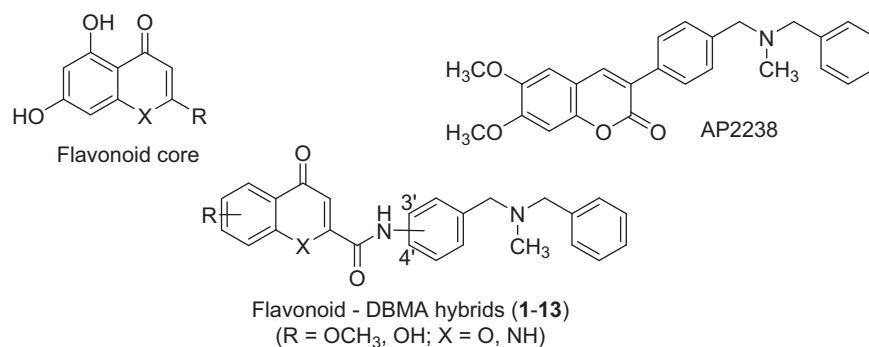
Figure 1. Structures of flavonoids, AP2238 and flavonoid − *N,N*-dibenzyl(*N*-methyl)amine hybrids (**1**–**13**).

array detector ($\lambda = 214$–274 nm), and using a Delta Pak C_{18} 5 μm, 300 Å column. The elution was performed in a gradient mixture of acetonitrile (ACN)/water, starting in most of cases with 15% and ending with 95% of ACN within 5 min (Water – ACN (1 5 →95%), g.t. 5 min). Melting points were determined in a MP70 apparatus (Mettler Toledo). ^{1}H NMR and ^{13}C NMR spectra were obtained in MeOD, DMSO-d$_6$ CDCl$_3$ or CD$_3$OD solutions using Varian INOVA-300, Varian INOVA-400, Varian Mercury-400 or Varian Unity-500 spectrometers. High resolution mass spectrometry (HRMS) data were obtained by electron spray ionisation in positive mode (ESI$^+$) using a Hewlett-Packard MSD 1100 spectrometer.

Synthesis of chromene – DBMA hybrids (general method A)

The corresponding 4-oxo-4*H*-chromene-2-carboxylic acid (1.0 mmol) and CDI (1.3 mmol) were mixed into a 10 ml mw vial under N$_2$ atmosphere. The vial was sealed up and 5 ml of anhydrous DMF were added using a syringe to dissolve the mixture (CO$_2$↑). This solution was heated into an mw reactor at 120 °C during 10 min to complete the activation of the acid. Afterward, a solution of the corresponding amine (1.2 mmol) in 2 ml of DMF was added with a syringe; this final solution was heated during 10 min at 150 °C to obtain the desired amide. After completion of the reaction, the DMF was evaporated under reduced pressure; the crude material was re-dissolved in 25 ml of EtOAc and washed with water (5 × 5 ml), brine (3 × 5 ml), dried over MgSO$_4$ and concentrated. The product was purified by column chromatography using EtOAc:MeOH (9:1) as eluent.

Synthesis of phenolic derivatives (method B)

Under N$_2$ atmosphere, to a solution of the corresponding methoxy hybrid (0.1 mmol) in anhydrous DCM (3 ml), BBr$_3$ (1 equivalent per each heteroatom present in the molecule) was added slowly under magnetic stirring. The mixture was allowed to react overnight at RT and then, quenched with MeOH (dropwise until end of effervescence). Solvent was evaporated under reduced pressure and MeOH addition was repeated several times until no fumes were observed. The residue was purified by column chromatography using a gradient of EtOAc/MeOH 0 → 10% as eluent.

Synthesis of 4-oxo-1,4-dihydroquinoline – DBMA hybrids (general method C)

Under N$_2$ atmosphere, to a mixture of the corresponding methyl 4-oxo-1,4-dihydroquinoline-2-carboxylate (1.0 mmol) and the corresponding amine (2.5 mmol) in dry THF (3.5 ml) in a mw vial, Al(CH$_3$)$_3$ (2 M in heptane, 3.0 mmol) was injected with a syringe. This mixture was heated into an mw reactor at 120 °C during

1.5 min and then, the crude material was treated with HCl 2 M (dropwise) until the end of gas generation, neutralised with NaOH 2 M and the liquid phase evaporated to dryness. The solid was washed with EtOAc (5 × 5.0 ml) and MeOH (2 × 5.0 ml) and these fractions were mixed and concentrated under reduced pressure. The product was purified by column chromatography using a gradient of EtOAc in hexane (0 → 65%) as eluent.

N-(4-((Benzyl(methyl)amino)methyl)phenyl)-6-methoxy-4-oxo-4*H*-chromene-2-carboxamide (1). White solid, yield: 77% (method A); mp 146-147 °C. ^{1}H NMR (300 MHz, CDCl$_3$) δ 8.55 (s, 1H, NH), 7.67 (d, $J = 8.5$ Hz, 2H, H$_{2'}$), 7.59 (d, $J = 3.1$ Hz, 1H, H$_5$), 7.54 (d, $J = 9.1$ Hz, 1H, H$_7$), 7.42 (d, $J = 8.5$ Hz, 2H, H$_{3'}$), 7.39 – 7.29 (m, 5H, H$_{8, o, m}$), 7.28 – 7.23 (m, 2H, H$_{3, p}$), 3.91 (s, 3H, 6-OMe), 3.54 (s, 2H, H$_\beta$), 3.53 (s, 2H, H$_\alpha$), 2.20 (s, 3H, H$_\gamma$) (Figure S1). ^{13}C NMR (75 MHz, CDCl$_3$) δ 178.02 (C$_4$), 157.78 (C$_6$), 157.06 (C$_9$), 154.52 (C$_2$), 150.02 (C$_{8a}$), 139.28 (C$_i$), 137.14 (C$_{4'}$), 135.26 (C$_{1'}$), 129.86 (C$_{3'}$), 129.05 (C$_m$), 128.39 (C$_p$), 127.13 (C$_o$), 125.24 (C$_{4a}$), 124.90 (C$_8$), 120.47 (C$_{2'}$), 119.60 (C$_7$), 111.84 (C$_3$), 105.34 (C$_5$), 61.99 (C$_\beta$), 61.37 (C$_\alpha$), 56.16 (C, 6-OMe), 42.37 (C$_\gamma$) (Figure S2). HRMS [ESI+] $m/z = 428.1754$ [M]$^+$, calculated for [C$_{26}$H$_{24}$N$_2$O$_4$]$^+$ 428.1736 (Figure S3). HPLC purity 99%.

N-(4-((Benzyl(methyl)amino)methyl)phenyl)-6-hydroxy-4-oxo-4*H*-chromene-2-carboxamide (2). Yellow solid, yield: 90% (method B); mp 186-189 °C. ^{1}H NMR (500 MHz, MeOD) δ 7.77 (d, $J = 8.6$ Hz, 2H, H$_{2'}$), 7.73 (d, $J = 9.1$ Hz, 1H, H$_8$), 7.45 (d, $J = 2.9$ Hz, 1H, H$_5$), 7.41 (d, $J = 8.6$ Hz, 2H, H$_{3'}$), 7.38 – 7.31 (m, 5H, H$_{7, o, m}$), 7.29 – 7.25 (m, 1H, H$_p$), 7.05 (s, 1H, H$_3$), 3.56 (s, 4H, H$_{\alpha, \beta}$), 2.20 (s, 3H, H$_\gamma$) (Figure S4). ^{13}C NMR (126 MHz, MeOD) δ 180.41 (C$_4$), 159.57 (C$_9$), 157.38 (C$_2$), 157.29 (C$_{8a}$), 151.03 (C$_6$), 139.51 (C$_i$), 137.75 (C$_{1'}$), 136.84 (C$_{4'}$), 130.92 (C$_o$), 130.42 (C$_{2'}$), 129.36 (C$_m$), 128.36 (C$_p$), 126.09 (C$_{4a}$), 125.57 (C$_7$), 122.39 (C$_{3'}$), 121.32 (C$_8$), 111.16 (C$_3$), 108.72 (C$_5$), 62.65 (C$_\beta$), 62.13 (C$_\alpha$), 42.30 (C$_\gamma$) (Figure S5). HRMS [ESI+] $m/z = 414.1583$ [M]$^+$, calculated for [C$_{25}$H$_{22}$N$_2$O$_4$]$^+$ 414.1580 (Figure S6). HPLC purity 100%.

N-(4-((Benzyl(methyl)amino)methyl)phenyl)-5,7-dimethoxy-4-oxo-4*H*-chromene-2-carboxamide (3). White solid, yield: 70% (method A); mp 99-101 °C. ^{1}H NMR (300 MHz, CDCl$_3$) δ 8.81 (s, 1H, NH), 7.88 (d, $J = 8.4$ Hz, 2H, H$_{2'}$), 7.60 (d, $J = 8.4$ Hz, 2H, H$_{3'}$), 7.56 – 7.41 (m, 5H, Ph), 7.26 (s, 1H, H$_3$), 6.75 (d, $J = 2.3$ Hz, 1H, H$_6$), 6.58 (d, $J = 2.3$ Hz, 1H, H$_8$), 4.11 (s, 3H, 7-OMe), 4.09 (s, 3H, 5-OMe), 3.73 (s, 2H, H$_\beta$), 3.72 (s, 2H, H$_\alpha$), 2.39 (s, 3H, H$_\gamma$) (Figure S7). ^{13}C NMR (75 MHz, CDCl$_3$) δ 176.96 (C$_4$), 164.84 (C$_7$), 161.28 (C$_5$), 159.02 (C$_{8a}$), 157.16 (C$_9$), 152.57 (C$_2$), 139.22 (C$_i$), 136.85 (C$_{4'}$), 135.48 (C$_{1'}$), 129.81 (C$_{3'}$), 129.05 (C$_o$), 128.38 (C$_m$), 127.13 (C$_p$), 120.47 (C$_{2'}$), 114.39 (C$_3$), 109.85 (C$_{4a}$), 96.86 (C$_6$), 93.03 (C$_8$), 61.94 (C$_\beta$), 61.37 (C$_\alpha$), 56.55 (C, 5-OMe), 56.05 (C, 7-OMe), 42.34 (C$_\gamma$) (Figure S8). HRMS [ESI+] $m/z = 458.1863$ [M]$^+$, calculated for [C$_{27}$H$_{26}$N$_2$O$_5$]$^+$ 458.1842 (Figure S9). HPLC purity 99%.

N-(4-((Benzyl(methyl)amino)methyl)phenyl)-5,7-dihydroxy-4-oxo-4H-chromene-2-carboxamide (4). Bright yellow solid, yield: 90% (method B); mp 199-200 °C. ^{1}H NMR (500 MHz, MeOD) δ 7.75 (d, $J = 8.5$ Hz, 2H, H$_{3'}$), 7.41 (d, $J = 8.5$ Hz, 2H, H$_{2'}$), 7.39 – 7.33 (m, 4H, H$_{o, m}$), 7.30 – 7.26 (m, 1H, H$_p$), 6.94 (s, 1H, H$_3$), 6.63 (d, $J = 2.1$ Hz, 1H, H$_8$), 6.28 (d, $J = 2.1$ Hz, 1H, H$_6$), 3.59 (s, 4H, H$_{\alpha, \beta}$), 2.22 (s, 3H, H$_\gamma$). ^{13}C NMR (126 MHz, MeOD) δ 183.60 (C$_4$), 167.44 (C$_7$), 163.42 (C$_5$), 159.15 (C$_9$), 159.00 (C$_{8a}$), 157.45 (C$_2$), 139.22 (C$_i$), 137.77 (C$_{4'}$), 136.59 (C$_{1'}$), 130.98 (C$_{2'}$), 130.48 (C$_o$), 129.40 (C$_m$), 128.46 (C$_p$), 122.50 (C$_{3'}$), 111.22 (C$_3$), 106.32 (C$_{4a}$), 100.92 (C$_6$), 95.94 (C$_8$), 62.60 (C$_\alpha$), 62.07 (C$_\beta$), 42.22 (C$_\gamma$). HRMS [ESI+] m/z = 430.1517 [M]$^+$, calculated for [C$_{25}$H$_{22}$N$_2$O$_5$]$^+$ 430.1529. HPLC purity 100%.

N-(4-((Benzyl(methyl)amino)methyl)phenyl)-6,7-dimethoxy-4-oxo-4H-chromene-2-carboxamide (5). White solid, yield: 80% (method A); mp 119-120 °C. ^{1}H NMR (300 MHz, MeOD) δ 7.89 (d, $J = 8.6$ Hz, 2H, H$_{3'}$), 7.53 – 7.35 (m, 9H, Ph, H$_{2', 5, 8}$), 7.06 (s, 1H, H$_3$), 4.04 (s, 3H, 6-OMe), 3.98 (bs, 4H, H$_{\alpha, \beta}$), 3.95 (s, 3H, 7-OMe), 2.49 (s, 3H, H$_\gamma$). ^{13}C NMR (75 MHz, MeOD) δ 179.39 (C$_4$), 159.50 (C$_9$), 157.48 (C$_6$), 156.76 (C$_2$), 153.49 (C$_{8a}$), 150.17 (C$_7$), 139.17 (C$_{4'}$), 136.52 (C$_{1'}$), 134.41 (C$_i$), 131.99 (C$_{2'}$), 131.33 (C$_o$), 129.93 (C$_m$), 129.84 (C$_p$), 122.53 (C$_{3'}$), 118.53 (C$_{4a}$), 111.87 (C$_3$), 104.71 (C$_5$), 101.48 (C$_8$), 61.77 (C$_\alpha$), 61.30 (C$_\beta$), 57.14 (C, 6-OMe), 56.69 (C, 7-OMe), 40.87 (C$_\gamma$). HRMS [ESI+] m/z = 458.1848 [M]$^+$, calculated for [C$_{27}$H$_{26}$N$_2$O$_5$]$^+$ 450.1842. HPLC purity 100%.

N-(3-((Benzyl(methyl)amino)methyl)phenyl)-6,7-dimethoxy-4-oxo-4H-chromene-2-carboxamide (6). White solid, yield: 90% (method A); mp 105-108 °C. ^{1}H NMR (400 MHz, MeOD) δ 7.79 (bs, 1H, H$_{2'}$), 7.71 (dd, $J = 8.2, 1.6$ Hz, 1H, H$_{4'}$), 7.46 (s, 1H, H$_5$), 7.39 – 7.31 (m, 6H, H$_{o, m, p, 8}$), 7.29 – 7.21 (m, 1H, H$_{5'}$), 7.20 (dt, $J = 8.2, 1.5$ Hz, 1H, H$_{6'}$), 7.03 (s, 1H, H$_3$), 4.01 (s, 3H, 6-OMe), 3.92 (s, 3H, 7-OMe), 3.55 (bs, 4H, H$_{\alpha, \beta}$), 2.19 (s, 3H, H$_\gamma$) (Figure S10). ^{13}C NMR (101 MHz, MeOD) δ 179.43 (C$_4$), 159.40 (C$_9$), 157.41 (C$_6$), 156.94 (C$_2$), 153.48 (C$_{8a}$), 150.11 (C$_7$), 140.93 (C$_i$), 139.68 (C$_{1'}$), 138.69 (C$_{3'}$), 130.40 (C$_o$), 129.89 (C$_p$), 129.34 (C$_m$), 128.29 (C$_{5'}$), 127.37 (C$_{6'}$), 123.17 (C$_{2'}$), 121.27 (C$_{4'}$), 118.50 (C$_{4a}$), 111.78 (C$_3$), 104.68 (C$_5$), 101.45 (C$_8$), 62.79 (C$_\alpha$), 62.57 (C$_\beta$), 57.10 (C, 6-OMe), 56.67 (C,/-OMe), 42.42 (C$_\gamma$) (Figure S11). HRMS [ESI+] m/z = 458.1840 [M]$^+$, calculated for [C$_{27}$H$_{26}$N$_2$O$_5$]$^+$ 458.1841 (Figure S12). HPLC purity 100%.

N-(4-((Benzyl(methyl)amino)methyl)phenyl)-5-methoxy-4-oxo-1,4-dihydroquinoline-2-carboxamide (7). White solid, yield: 60% (method C); mp 263-265 °C. ^{1}H NMR (500 MHz, CDCl$_3$) δ 10.20 (s, 1H NH$_{10}$), 9.88 (s, 1H, NH$_1$), 7.80 (d, $J = 8.3$ Hz, 2H, H$_{2'}$), 7.75 (s, 1H, H$_3$), 7.73 (m, 1H, H$_8$), 7.63 (t, $J = 7.8$ Hz, 1H, H$_7$), 7.46 – 7.36 (m, 4H, H$_{3', o}$), 7.34 (t, $J = 7.5$ Hz, 2H, H$_m$), 7.29 – 7.26 (m, 1H, H$_p$), 6.92 (dd, $J = 7.8, 0.9$ Hz, 1H, H$_6$), 4.13 (s, 3H, 5-OMe), 3.57 (s, 4H, H$_{\alpha, \beta}$), 2.23 (s, 3H, H$_\gamma$) (Figure S13). ^{13}C NMR (126 MHz, CDCl$_3$) δ 164.19 (C$_4$), 162.09 (C$_9$), 156.07 (C$_5$), 152.06 (C$_2$), 149.81 (C$_{8a}$), 136.90 (C$_{4'}$), 135.49 (C$_{1'}$), 130.07 (C$_7$), 129.88 (C$_{3'}$), 129.23 (C$_o$), 128.45 (C$_m$), 127.25 (C$_p$), 1213.37 (C$_8$), 119.77 (C$_{2'}$), 112.61 (C$_{4a}$), 105.39 (C$_6$), 104.34 (C$_3$), 61.84 (C$_\alpha$), 61.49 (C$_\beta$), 56.76 (C$_{51}$), 42.24 (C$_\gamma$) (Ci not detected) (Figure S14). HRMS [ESI+] m/z = 427.1900 [M]$^+$, calculated for [C$_{26}$H$_{25}$N$_3$O$_3$]$^+$ 427.1896 (Figure S15). HPLC purity 99%.

N-(4-((Benzyl(methyl)amino)methyl)phenyl)-6-methoxy-4-oxo-1,4-dihydroquinoline-2-carboxamide (8). White solid, yield: 60% (method C); mp 261-263 °C. ^{1}H NMR (500 MHz, DMSO-d$_6$) δ 10.61 (s, 1H, NH), 7.96 (d, $J = 9.1$ Hz, 1H$_8$), 7.82 (d, $J = 8.0$ Hz, 2H, H$_{2'}$), 7.49 (d, $J = 2.9$ Hz, 1H, H$_5$), 7.40 (dd, $J = 9.1, 2.9$ Hz, 1H, H$_7$), 7.38 – 7.30 (m, 7H, H$_{3, 3', o, m}$), 7.28 – 7.23 (m, 1H, H$_p$), 3.89 (s, 3H, 6-OMe), 3.50 (s, 2H, H$_\beta$), 3.48 (s, 2H, H$_\alpha$), 2.08 (s, 3H, H$_\gamma$) (Figure S16). ^{13}C NMR (126 MHz, DMSO-d$_6$) δ 157.07 (C$_6$), 139.09 (C$_i$), 136.99 (C$_{1'}$), 134.98 (C$_{4'}$), 128.98 (C$_{3'}$), 128.60 (C$_m$), 128.20 (C$_o$), 126.88 (C$_p$), 122.98 (C$_7$), 120.18 (C$_{2'}$), 60.97 (C$_\beta$), 60.57 (C$_\alpha$), 55.43 (C, 6-OMe),

41.63 (C$_\gamma$) (C$_3$ and quaternary carbons of 4-oxo-1,4-dihydroquinoline ring not detected) (Figure S17). HRMS [ESI+] m/z = 427.1905 [M]$^+$, calculated for [C$_{26}$H$_{25}$N$_3$O$_3$]$^+$ 427.1896 (Figure S18). HPLC purity 99%.

N-(4-((Benzyl(methyl)amino)methyl)phenyl)-6-hydroxy-4-oxo-1,4-dihydroquinoline-2-carboxamide (9). White solid, yield: 90% (method B); mp 248-251 °C. ^{1}H NMR (300 MHz, DMSO-d$_6$) δ 10.56 (s, 1H, NH), 7.90 (s, 1H), 7.82 (d, $J = 8.3$ Hz, 2H), 7.53 – 7.15 (m, 10H), 3.50 (s, 2H, CH$_2$), 3.48 (s, 2H, CH$_2$), 2.08 (s, 3H, CH$_3$) (Figure S19). ^{13}C NMR (75 MHz, DMSO-d$_6$) δ 139.08 (C), 137.00 (C), 128.96 (CH), 128.58 (CH), 128.18 (CH), 126.86 (CH), 122.80 (CH), 120.14 (CH), 60.95 (CH$_2$), 60.56 (CH$_2$), 41.61(CH$_3$) (Only one CH from the 4-chromenone system was detected in ^{13}C NMR) (Figure S20). HRMS [ESI+] m/z = 413.1751 [M]$^+$, calculated for [C$_{25}$H$_{23}$N$_3$O$_3$]$^+$ 413.1739 (Figure S21). HPLC purity 99%.

N-(4-((Benzyl(methyl)amino)methyl)phenyl)-7-methoxy-4-oxo-1,4-dihydroquinoline-2-carboxamide (10). White solid, yield: 62% (method C); mp 261-263 °C. ^{1}H NMR (300 MHz, DMSO-d$_6$) δ 11.73 (s, 1H, NH$_1$), 10.63 (s, 1H, NH$_{10}$), 8.01 (d, $J = 9.0$ Hz, 1H, H$_5$), 7.79 (d, $J = 8.1$ Hz, 2H, H$_{3'}$), 7.50 – 7.42 (m, 1H, H$_8$), 7.40 – 7.29 (m, 6H, H$_{2', o, m}$), 7.28 – 7.19 (m, 1H, H$_p$), 6.99 (bs, 1H, H$_6$), 6.86 (bs, 1H, H$_3$), 3.87 (s, 3H, 7-OMe), 3.50 (s, 2H, H$_\beta$), 3.49 (s, 2H, H$_\alpha$), 2.08 (s, 3H, H$_\gamma$). ^{13}C NMR (75 MHz, DMSO-d$_6$) δ 177.03 (C$_4$), 162.28 (C$_7$), 160.65 (C$_9$), 139.04 (C$_i$), 136.88 (C$_{4'}$), 135.22 (C$_{1'}$), 128.98 (C$_{2'}$), 128.59 (C$_m$), 128.18 (C$_o$), 126.87 (C$_p$), 126.44 (C$_5$), 120.43 (C$_{3'}$), 113.96 (C$_6$), 107.56 (C$_3$), 100.31 (C$_8$), 60.96 (C$_\beta$), 60.53 (C$_\alpha$), 55.45 (C, 7-OMe), 41.59 (C$_\gamma$). HRMS [ESI+] m/z = 427.1898 [M]$^+$, calculated for [C$_{26}$H$_{25}$N$_3$O$_3$]$^+$ 427.1896. HPLC purity 99%.

N-(4-((benzyl(methyl)amino)methyl)phenyl)-6,7-dimethoxy-4-oxo-1,4-dihydroquinoline-2-carboxamide (11). White solid, yield: 35% (method C); mp 245-248 °C. ^{1}H NMR (500 MHz, MeOD) δ 7.79 (d, $J = 8.2$ Hz, 2H, CH), 7.59 (s, 1H, CH), 7.42 (d, $J = 8.2$ Hz, 2H, CH), 7.48 – 7.25 (m, 7H,), 7.05 (bs, 1H, NH), 4.00 (s, 3H, Me), 3.96 (s, 3H, OMe), 3.70 (bs, 4H, 2xCH$_2$), 2.30 (s, 3H, CH$_3$). ^{13}C NMR (126 MHz, MeOD) δ 156.16 (C), 150.33 (C), 138.73 (C), 137.98 (C), 134.68 (C), 131.33 (CH), 130.76 (CH), 129.57 (CH), 128.89 (CH), 122.06 (CH), 103.89 (CH), 62.32 (CH), 61.85 (CH), 56.70 (C, OMe), 56.48 (C, OMe), 41.82 (CH$_3$) (Some CH's and quaternary carbons were not detected). HRMS [ESI+] m/z = 457.2009 [M]$^+$, calculated for [C$_{27}$H$_{27}$N$_3$O$_4$]$^+$ 457.2002. HPLC purity 99%.

N-(4-((benzyl(methyl)amino)methyl)phenyl)-6,7-dihydroxy-4-oxo-1,4-dihydroquinoline-2-carboxamide (12). White solid, yield: 90% (method B); mp 248-251 °C. ^{1}H NMR (500 MHz, MeOD) δ 7.99 (d, $J = 8.1$ Hz, 2H, H$_{2'}$), 7.64 (d, $J = 8.1$ Hz, 2H, H$_{3'}$), 7.62 (s, 1H, H$_3$), 7.60 – 7.55 (m, 2H, H$_m$), 7.54 – 7.50 (m, 5H, H$_{5, 8, o, p}$), 4.58 – 4.51 (m, 2H, H$_\alpha$), 4.39 – 4.30 (m, 2H, H$_\beta$), 2.77 (s, 3H, H$_\gamma$). ^{13}C NMR (126 MHz, MeOD) δ 194.03 (C$_4$), 170.55 (C$_9$), 160.79 (C), 156.94 (C$_7$), 150.15 (C$_6$), 143.73 (C), 140.71 (C$_{1'}$), 133.97 (C), 133.26 (C$_{3'}$), 132.39 (C$_o$), 131.31 (C$_p$), 130.77 (C$_i$), 130.45 (C$_m$), 127.38 (C$_{4'}$), 122.65 (C$_{2'}$), 118.34 (C$_8$), 111.41 (C), 105.80 (C$_3$), 103.76 (C$_5$), 60.76 (C$_\alpha$), 60.30 (C$_\beta$), 39.55 (C$_\gamma$). HRMS [ESI+] m/z = 429.1700 [M]$^+$, calculated for [C$_{25}$H$_{23}$N$_3$O$_4$]$^+$ 429.1689. HPLC purity 99%.

N-(3-((Benzyl(methyl)amino)methyl)phenyl)-6,7-dimethoxy-4-oxo-1,4-dihydroquinoline-2-carboxamide (13). White solid, yield: 90% (method C); mp 131–133 °C. ^{1}H NMR (500 MHz, MeOD) δ 7.92 (s, 1H, CH), 7.76 (dd, $J = 7.6, 1.3$ Hz, 1H, CH), 7.55 (s, 1H, CH), 7.50 – 7.38 (m, 7H, Ph, 2xCH,), 7.31 (s, 1H, CH), 7.27 (dt, $J = 7.7, 1.3$ Hz, 1H, CH), 4.04 – 4.00 (bs, 4H, 2xCH$_2$), 3.99 – 3.98 (m, 3H, OMe), 3.94 (s, 3H, OMe), 2.51 (s, 3H, CH$_3$) (Figure S22). ^{13}C NMR (126 MHz, MeOD) δ 156.08 (C), 150.35 (C), 139.66 (CH), 131.43 (CH), 130.54 (CH), 129.98 (CH), 129.98 (CH), 127.84 (CH), 123.80 (CH), 122.42 (CH), 103.75 (CH), 61.75 (CH$_2$), 61.58 (CH$_2$), 56.68 (C, OMe), 56.45 (C, OMe), 41.00 (CH$_2$) (Quaternary carbons not observed and just

one CH from the 4-chromenone system detected in ^{13}C NMR) (Figure S23). HRMS [ESI+] $m/z = 457.2002$ [M]$^+$, calculated for [C$_{27}$H$_{27}$N$_3$O$_3$]$^+$ 457.2001 (Figure S24). HPLC purity 99%.

Biochemical studies

Inhibition of human acetyl- and butyrylcholinesterase (hAChE and hBuChE)

The Ellman method was followed, using human recombinant AChE and BuChE from human serum[48]. The assay solution consisted of 0.1 M phosphate buffer pH 8.0, 400 μM 5,5′-dithiobis(2-nitrobenzoic acid) (DTNB, Ellman's reagent), 0.05 U/mL hAChE (Sigma Chemical Co.) or 0.024 U/mL hBuChE (Sigma Chemical Co.), and 800 μM acetylthiocholine iodide, or 500 μM butyrylthiocholine as the substrate of the enzymatic reaction, respectively. The compounds tested were added to the assay solution and preincubated with the enzyme for 5 min at 30 °C. After that period, the substrate was added. The absorbance changes at 412 nm were recorded for 5 min with a UV/Vis microplate spectrophotometer, Multiskan Spectrum, Thermo-Electron Co. The reaction rates were compared and the inhibition percentage due to the presence of test compound was calculated. The IC$_{50}$ is defined as the concentration of each compound that reduces at 50% the enzymatic activity without any inhibitor.

Inhibition of human monoamine oxidases (hMAO-A and hMAO-B)

MAO inhibition measurements were evaluated following the general procedure previously described[49]. Briefly, test drugs and adequate amounts of recombinant hMAO-A or hMAO-B (Sigma-Aldrich, Spain) required and adjusted to oxidise 165 pmol of p-tyramine/min in the control group, were incubated for 15 min at 37 °C in a flat-black-bottom 96-well microtest plate (BD Biosciences, Franklin Lakes, NJ) placed in the dark fluorimeter chamber. The reaction was started by adding 200 mM Amplex Red reagent (Molecular Probes, Inc., Eugene, OR), 1 U/mL horseradish peroxidase, and 1 mM p-tyramine. Then, the production of resorufin was quantified at 37 °C in a multidetection microplate fluorescence reader (FLX800, Bio-Tek Instruments, Inc., Winooski, VT) based on the fluorescence generated (excitation, 545 nm; emission, 590 nm). The specific fluorescence emission was calculated after subtraction of the background activity, which was determined from wells containing all components except the hMAO isoforms, which were replaced by a sodium phosphate buffer solution.

Oxygen radical absorbance capacity assay (ORAC)

Antioxidant activities were measured using the ORAC method[50], in a Polarstar Galaxy plate reader (BMG Labtechnologies GmbH, Offenburg, Germany) with 485-P excitation and 520-P emission filters. The equipment was controlled by the Fluorostar Galaxy software (version 4.11–0) for fluorescence measurement. 2,2′-Azobis-(amidinopropane) dihydrochloride (AAPH), (±)-6-hydroxy-2,5,7,8-tetramethylchromane-2-carboxylic acid (trolox) and fluorescein (FL) were purchased from Sigma-Aldrich. The reaction was carried out in 75 mM phosphate buffer (pH 7.4) and the final reaction mixture was 200 μL. Antioxidant (20 μL) and FL (120 μL; 70 mM, final concentration) solutions were placed in a black 96-well microplate (96 F untreat, Nunc). The mixture was pre-incubated for 15 min at 37 °C and then, AAPH solution (60 μL, 12 mM, final concentration) was added rapidly using a multichannel pipette. The microplate was immediately placed in the reader and the fluorescence was recorded every minute for 80 min. The microplate was automatically shaken prior each reading. Samples were measured at eight different concentrations (0.1–1 μM). A blank (FL + AAPH in phosphate buffer) instead of the sample solution and eight calibration solutions using trolox (1–8 μM) were also carried out in each assay. All the reaction mixtures were prepared in duplicate, and at least three independent assays were performed for each sample. Raw data were exported from the Fluostar Galaxy Software to an Excel sheet for further calculations. Antioxidant curves (fluorescence vs. time) were first normalised to the curve of the blank corresponding to the same assay, and the area under the fluorescence decay curve (AUC) was calculated. The net AUC corresponding to a sample was calculated by subtracting the AUC corresponding to the blank. Regression equations between net AUC and antioxidant concentration were calculated for all the samples. ORAC values were expressed as trolox equivalents by using the standard curve calculated for each assay, where the ORAC value of trolox was taken as 1.0.

In vitro blood–brain barrier permeation assay (PAMPA-BBB)

Prediction of the brain penetration was evaluated using a parallel artificial membrane permeation assay (PAMPA-BBB), in a similar manner as previously described[36,46,51–53]. Pipetting was performed with a semi-automatic pipettor (CyBi®-SELMA) and UV reading with a microplate spectrophotometer (Multiskan Spectrum, Thermo Electron Co.). Commercial drugs, phosphate buffered saline solution at pH 7.4 (PBS), and dodecane were purchased from Sigma, Aldrich, Acros, and Fluka. Millex filter units (PVDF membrane, diameter 25 mm, pore size 0.45 μm) were acquired from Millipore. The porcine brain lipid (PBL) was obtained from Avanti Polar Lipids. The donor microplate was a 96-well filter plate (PVDF membrane, pore size 0.45 μm) and the acceptor microplate was an indented 96-well plate, both from Millipore. The acceptor 96-well microplate was filled with 200 μL of PBS: ethanol (70:30) and the filter surface of the donor microplate was impregnated with 5 μL of porcine brain lipid (PBL) in dodecane (20 mg mL^{-1}). Compounds were dissolved in PBS: ethanol (70:30) at 100 μg mL^{-1}, filtered through a Millex filter, and then added to the donor wells (200 μL). The donor filter plate was carefully put on the acceptor plate to form a sandwich, which was left undisturbed for 120 min at 25 °C. After incubation, the donor plate is carefully removed and the concentration of compounds in the acceptor wells was determined by UV-Vis spectroscopy. Every sample is analysed at five wavelengths, in four wells and at least in three independent runs, and the results are given as the mean ± standard deviation. In each experiment, 11 quality control standards of known BBB permeability were included to validate and normalise the analysis set.

Human BACE-1 inhibition assay

This experiment was carried out according to the protocol described by the manufacturer (Invitrogen) using a FRET assay[54]. Briefly, an APP-based peptide substrate (rhodamine-EVNLDAEFK-quencher, Km of 20 μM) carrying the Swedish mutation and containing a rhodamine as a fluorescence donor and a quencher acceptor at each end was used. The intact substrate is weakly fluorescent and becomes highly fluorescent upon enzymatic cleavage. The assays were conducted in 50 mM sodium acetate buffer, pH 4.5, in a final enzyme concentration (1 U/mL). The mixture was incubated for 60 min at 25 °C under dark conditions and then stopped with 2.5 M sodium acetate. Fluorescence was measured with a FLUOstar Optima (BMG Labtechnologies GmbH,

Offenburg, Germany) microplate reader at 545 nm excitation and 585 nm emission.

Inhibition of human lipoxygenase-5 (hLOX-5)

The fluorescence-based enzyme method developed by Pufahl et al. was followed[55], in 96-well microtiter plates. The assay solution consists of Tris buffer (50 mM, pH 7.5), ethylenediaminetetraacetic acid (EDTA, 2 mM), $CaCl_2$ (2 mM), arachidonic acid (AA, 3 μM), ATP (10 μM), 2′,7′-dichlorodihydrofluorescein diacetate (H_2DCFDA, 10 μM), hLOX-5 (100 mU/well), bovine glutathione peroxidase (GPx, 25 mU/well) and reduced glutathione (GSH, 1 mM). Compounds to be tested were added to the test solution prior to AA and ATP, and pre-incubated for a period of 10 min at room temperature. Then, the AA and ATP substrates were added; the enzymatic reaction allowed to progress for 20 min and ended by the addition of 40 μL of acetonitrile. The fluorescence measurements (excitation: 485 nm; emission: 520 nm) were performed on a FLUOstar OPTIMA (BMG LABTECH, Offenburg, Germany). IC_{50} is defined as the concentration of compound that inhibits enzymatic activity by 50% over the control of untreated enzyme.

Binding assays at sigma-1 and sigma-2 receptors

For σ_1R assay, the thawed membrane preparation of guinea pig brain cortex (about 100 μg of protein) were incubated for 120 min at 37 °C with 2 nM [^{3}H]-(+)-pentazocine (PerkinElmer, specific activity 34.9 C_i/mmol) in 50 mM Tris-HCl, pH 7.4, 0.5 ml final volume. Non-specific binding was defined in the presence of 10 μM of unlabelled (+)-pentazocine. The reaction was stopped by vacuum filtration through GF/B glass-fiber filters presoaked with 0.5% polyethylenimine, followed by rapid washing with 2 ml ice-cold buffer. Filters were placed in 3 ml scintillation cocktail and the radioactivity determined by liquid scintillation counting.

For σ_2R assay, 150 μg of rat liver homogenate were incubated for 120 min at room temperature with 3 nM [^{3}H]-DTG (PerkinElmer, specific activity 58.1 C_i/mmol) in 50 mM Tris-HCl, pH 8.0, 0.5 ml final volume. (+)-Pentazocine (500 nM) was used to mask σ_1R and to define non-specific binding, respectively.

Competition studies were done using at least 11 different concentrations of the ligand under investigation. As control, three increasing concentrations of unlabeled (+)-pentazocine (σ_1R) or DTG (σ_2R) were always included. The compounds were prepared as 10 mM stock solutions in 100% DMSO and diluted with Tris-HCl buffer on the day of the experiment. The final DMSO concentration in the incubation tubes was maintained at 0.1%[56].

IC_{50} values and Hill's coefficients n_H were calculated by nonlinear regression using a four parameters curve-fitting algorithm of the GraphPad Prism software (v(0).6, La Jolla California USA), and are reported as the mean ± SEM of three separate determinations performed in duplicate. The corresponding K_i values were obtained by means of the Cheng–Prusoff equation, using the K_d values obtained in saturation experiments.

Molecular simulation details

All simulations were carried out using the Pmemd modules of Amber 18[57], running on our own CPU/GPU calculation cluster. Molecular graphics images were produced using the UCSF Chimera package (v.1.10)[58]. All other graphs were obtained using GraphPad Prism (v. 6.0). The molecular structures of hAChE, of hLOX-5, and of hBACE-1 were obtained from the Protein Data Bank (pdb code: 4EY7[59], pdb code: 3V99[60], and pdb code: 1M4H[61] respectively) while the optimised membrane-bound 3 D structure

of the σ_1 receptor was obtained starting from the available Protein Data Bank file (pdb code: 5HK1[62]) and following a procedure previously described[63,64].

The optimised structures of **6** were docked into each protein identified binding pocket using Autodock 4.2.6/Autodock Tools 1.4.6[65] on a win64 platform. The resulting docked conformations were clustered and visualised; then, the structure of each resulting complex characterised by the lowest Autodock interaction energy in the prevailing cluster was selected for further modeling. Each compound/protein complex obtained from the docking procedure was further refined in Amber 18 using the quenched molecular dynamics (QMD) method as previously described [see, for example[32,66–68], and reference therein]. Next, the best energy configuration of each complex resulting from QMD was subsequently solvated by a cubic box of TIP3P water molecules[69] extending at least 10 Å in each direction from the solute. The system was neutralised and the solution ionic strength was adjusted to the physiological value of 0.15 M by adding the proper amounts of Na^+ and Cl^- ions. Each solvated system was relaxed (500 steps of steepest descent followed by 500 other conjugate-gradient minimisation steps) and then gradually heated to the target temperature of 298 K in intervals of 50 ps of constant volume-constant temperature (NVT) molecular dynamics (MD) simulations (Verlet integration method, time step 1.0 fs). The Langevin thermostat was used to control temperature. During this phase of MD, the protein was restrained with a force constant of 2.0 kcal/(mol Å), and all simulations were carried out with periodic boundary conditions. Subsequently, the density of the system was equilibrated via MD runs in the isothermal-isobaric (NPT) ensemble, with a time step of 1 fs. All restraints on the protein atoms were then removed, and each system was further equilibrated using NPT MD runs at 298vK. Three equilibration steps were performed (4 ns each, time step 2.0 fs). System stability was monitored by the fluctuations of the root-mean-square-deviation (RMSD) of the simulated position of the backbone atoms of the protein with respect to those of the initial protein model. The equilibration phase was followed by a data production run consisting of 50 ns of MD simulations in the NVT ensemble. Data collection was performed on over the last 20 ns of each equilibrated MD trajectory were considered for statistical data collections. 1000 trajectory snapshots were analysed for each **6**/receptor complex. The free energy of binding ΔG_{bind} between **6** and the target proteins was estimated by resorting to the well-validated Molecular Mechanics/Poisson–Boltzmann Surface Area (MM/PBSA) approach[70] implemented in Amber 18. The per residue binding free energy decomposition (interaction spectra) was carried out using the Molecular Mechanics/Generalized Boltzmann Surface Area (MM/GBSA) approach[71,72], and was based on the same snapshots used in the binding free energy calculation.

Study of theoretical medicinal chemistry alerts in free databases

SMILES code of hybrids **1**–**13** were uploaded in two databases, namely ZINC15 (http://zinc15.docking.org/)[73] and SwissADME (http://www.swissadme.ch/)[74]. PAINs and aggregation results are gathered in Table S1 (Supplementary information).

Neurogenic assays

Adult (3 months old) male C57BL/6 mice were used following the animal experimental procedures previously approved by the Ethics Committee for Animal Experimentation of the CSIC in accordance with the European Communities Council, directive 2010/63/EEC and National regulations, normative 53/2013. Special care was

taken to minimise animal suffering. Neural stem cells were isolated from the SGZ of the dentate gyrus of the hippocampus of adult mice and cultured as NS according to previously published protocols[75,76]. Neural stem cells grown as NS were treated for 7 days in culture with compound **6** (10 μM). Now, NS were adhered onto 100 μg/mL poly-L-lysine-coated coverslips and treated for 3 additional days in the presence of serum but in the absence of exogenous growth factors to induce differentiation[77]. Finally, the expression of neuronal markers was analysed by immunocytochemistry using antibodies linked to neurogenesis: β-III-tubulin polyclonal antibody (TuJ clone; Abcam), a protein expressed at early stages of neurogenesis and a monoclonal microtubule-associated protein type 2 (MAP-2) antibody, a classical marker of late neuronal maturation. To visualise primary antibodies Alexa-fluor-labeled secondary antibodies (Molecular probes) were used. Nuclei were stained with DAPI. Fluorescent representative images were acquired in a LSM710 laser scanning spectral confocal microscope (Zeiss). Confocal microscope settings were adjusted to produce the optimum signal-to-noise ratio.

In silico toxicity and metabolism predictions

To assess toxicity prediction, we use Derek Nexus v 6.0.1 (knowledge base 2018 1.1, species: human), which is a knowledge-based expert system by Lhasa Limited where toxicity predictions consider the presence of a toxicophore in the query structure, and are the result of two processes: evaluating alerts and estimating the likelihood of toxicity[78]. The likelihood levels in Derek Nexus in highest to lowest order are: certain, probable, plausible, equivocal, doubted, improbable, and impossible[79].

To predict metabolism, we use Meteor Nexus v 3.1.0 (knowledge base 2018 1.0.0), a knowledge-based approach to rank metabolites based on known metabolic reactions[78]. To predict first metabolic step of the parent compound (hybrid **6**), we analysed the phase-I biotransformation pathways, combining two different methods[80]. A qualitative [absolute reasoning (AR)] and quantitative (site of metabolism (SOM) scoring) assessment was applied, selecting the matching metabolites. The AR evaluated the likelihood level for a biotransformation to occur, and the minimal likelihood level was settled in "plausible", what means that the weight of evidence supports the proposition[79]. The SOM scoring method uses experimental data for compounds that match the same biotransformation, have similar molecular weights and are chemically similar around the site of metabolism to hybrid **6**.

Mutagenic and carcinogenic risk assessment

The International Conference on Harmonisation (ICH) of technical requirements for registration of pharmaceuticals for human use has developed a guideline for the assessment and control of mutagenic impurities to limit potential carcinogenic risk, ICH M7[81]. This guideline purposes to provide a framework to identify mutagenic alerts with computational toxicology assessment, it has to be performed using two complementary QSAR methodologies. To reach this objective, we have used an *in silico* prediction system from Lhasa ltd. (Leeds, UK), Derek Nexus v3.2.0 (expert rule-based methodology) and Sarah Nexus v3.0.0 (statistical-based methodology) to obtain a classification according to OECD Guidance Document on the Validation of (Q)SAR Models[82].

Results and discussion

Chemistry

The common precursors for synthesising desired hybrids **1–13** were 3- or 4-((benzyl(methyl)amino)methyl)anilines (Figure 2), which were obtained in excellent yields following well-known procedures. The coupling reaction between the above-mentioned anilines and several substituted 4-oxo-4H-chromene-2-carboxylic acids, in a microwave oven (mw) at 120 °C, using 1,1′-carbonyldiimidazole (CDI) as activating agent, gave 4-chromenone hybrids **1**, **3**, **5**, and **6** in good yields (70–90%). The methoxy-bearing 4-quinolinone hybrids (**7**, **8**, **10**, **11**, and **13**) were obtained in 50–90% yield by the Al(CH$_3$)$_3$-mediated amide formation between the corresponding aniline precursor and several substituted methyl 4-oxo-1,4-dihydroquinoline-2-carboxylates, into a mw oven at 120 °C. Finally, hydroxyl substituted compounds (**2**, **4**, **9**, and **12**) were obtained by the overnight treatment of the corresponding methoxy derivative with BBr$_3$ in THF at RT. For achieving good yields in these transformations (70–90%) it was necessary to use one BBr$_3$ equivalent for each ether group to be cleavage plus an additional equivalent for each heteroatom present in the molecule, due to the well-known complexation ability of the boron atom[52,83].

All 4-chromenone – and 4-quinolone – DBMA hybrids **1–13** were purified in silica gel cartridges using an automatic chromatographic equip (IsoleraOne, Biotage) and were characterised by their analytical (HPLC, HRMS) and spectroscopic data (¹H NMR, ¹³C NMR). Complete NMR assignment of their hydrogen and carbon atoms were made by ¹H – ¹³C two-dimensional diagrams, mainly
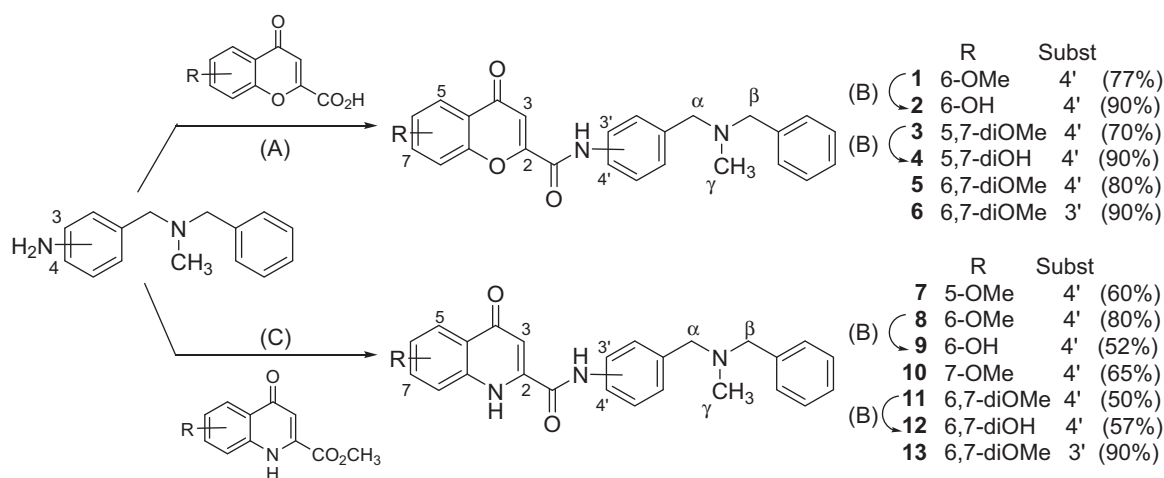

Figure 2. Synthesis of flavonoid – *N,N*-dibenzyl(*N*-methyl)amine hybrids (**1–13**). Reagents and conditions: (A) CDI, DMF, mw 120 °C, 10 min; (B) BBr$_3$, DCM, r.t., overnight; (C) Al(CH$_3$)$_3$, THF, mw 120 °C, 3 min.

HSQC (heteronuclear single quantum correlation) and HMBC (heteronuclear multiple bond correlation).

substituents ranked as follows: 6-hydroxy $\geq$ 6-methoxy $\geq$ 5,7-dihydroxy > 5,7-dimethoxy.

Inhibition of human cholinesterases

Firstly, new hybrids **1**–**13** were tested as inhibitors of human cholinesterases, namely hAChE and hBuChE, following the Ellman method and using donepezil as reference drug[48]. As shown in Table 1, new hybrids are potent and selective inhibitors of hAChE, with IC_{50} values comprised between the one-digit-micromolar and the sub-micromolar range. In all cases, the inhibition of hBuChE was worse, with IC_{50} exceeding 10 μM. Chromone derivatives displayed better hAChE inhibition potencies than their 4-quinolone counterparts (e.g. compare the pairs **1** vs. **8**; **2** vs. **9**; **5** vs. **11**; **6** vs. **13**). The nature of the substituents in the 4-chromenone ring exerted only modest effects on the hAChE inhibition; from the most effective hybrid **5** (IC_{50}=0.99 μM) derived from 6,7-dimethoxy-4-oxo-4H-chromene, the inhibitory potencies given by the

Inhibition of human monoamine oxidases and antioxidant properties

New 4-chromenone – DBMA and 4-quinolone – DBMA hybrids (**1**–**13**) were evaluated as inhibitors of human recombinant MAO's, expressed in baculovirus containing cDNA inserts for hMAO-A and hMAO-B. The production of oxygen peroxide from a common substrate for both isoenzymes (p-tyramine) was quantified using the Amplex Red MAO assay kit[84] and results are gathered in Table 1. Five derivatives inhibited hMAO's in the micromolar range, whereas the rest of tested compounds were found to be inactive at 100 μM (the highest concentration tested). All active hybrids, displayed higher potency towards hMAO-A than several drugs currently in clinical use for treating AD, PD and depressive

Table 1. Inhibition of human acetylcholinesterase (hAChE) and human monoamine oxidases (hMAO-A and hMAO-B). Assessment of the oxygen radical absorbance capacity (ORAC, trolox equivalents) and the CNS-permeation (PAMPA-BBB assay).

Compd.	X	R	Substitution	hAChE[a]	hMAO-A[a]	hMAO-B[a]	ORAC[b]	PAMPA-BBB[c]
1	O	6-OMe	4′	1.5 ± 0.2	1.6 ± 0.4	59.8 ± 3.7	n.d.	17.1 ± 1.5
2	O	6-OH	4′	1.3 ± 0.3	7.0 ± 0.8	9.7 ± 1.6	1.6 ± 0.2	6.8 ± 0.4
3	O	5,7-diOMe	4′	3.2 ± 0.4	>100	>100	n.d.	19.4 ± 1.7
4	O	5,7-diOH	4′	1.9 ± 0.6	22.8 ± 1.5	>100	1.2 ± 0.1	14.7 ± 1.2
5	O	6,7-diOMe	4′	1.0 ± 0.2	9.0 ± 0.1	8.1 ± 0.4	n.d.	19.1 ± 1.5
6	O	6,7-diOMe	3′	4.5 ± 0.8	>100	>100	n.d.	18.8 ± 1.3
7	NH	5-OMe	4′	4.0 ± 0.4	>100	15.2 ± 1.0	n.d.	23.0 ± 2.1
8	NH	6-OMe	4′	2.3 ± 0.1	>100	>100	n.d.	24.8 ± 2.0
9	NH	6-OH	4′	3.1 ± 0.3	>100	>100	1.2 ± 0.1	8.4 ± 0.7
10	NH	7-OMe	4′	2.3 ± 0.2	>100	>100	n.d.	21.7 ± 1.9
11	NH	6,7-diOMe	4′	4.5 ± 0.3	>100	>100	n.d.	19.1 ± 1.5
12	NH	6,7-diOH	4′	>10	>100	>100	0.5 ± 0.1	8.8 ± 0.7
13	NH	6,7-diOMe	3′	>10	>100	>100	n.d.	15.1 ± 1.2
Donepezil				0.01 ± 0.002	n.d.	n.d.	n.d.	n.d.
(R)-Deprenyl				n.d.	68.7 ± 4.2	0.017 ± 0.002	n.d.	n.d.
Iproniazid				n.d.	6.7 ± 0.8	7.5 ± 0.4	n.d.	n.d.
Moclobemide				n.d.	161.4 ± 19.4	>100	n.d.	n.d.
Trolox				n.d.	n.d.	n.d.	1.0	n.d.

Results are expressed as the mean ± SEM ($n = 3$).
[a]IC_{50} (μM).
[b]Trolox equivalents (mmol of trolox/mmol of tested compound).
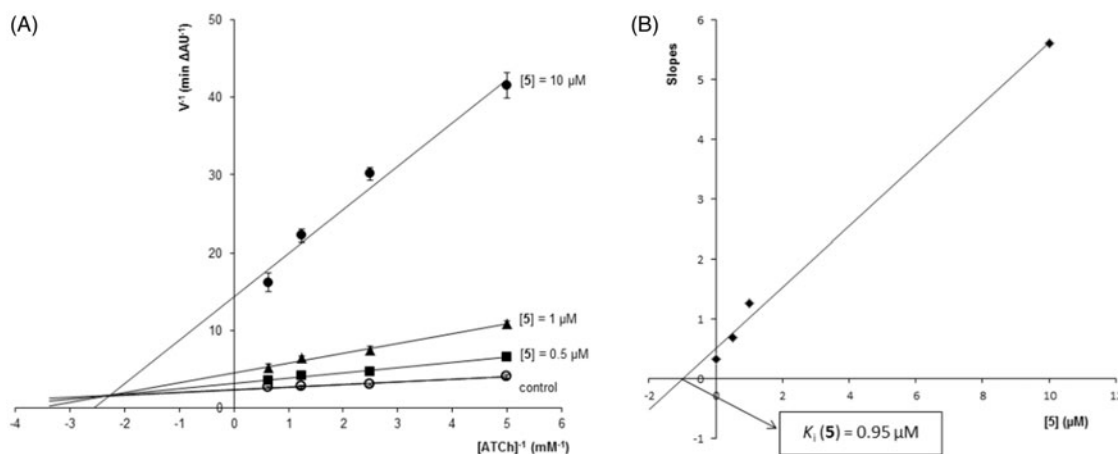[c]Permeability in the CNS (P_e, 10^{-6} cm s^{-1}).

Figure 3. Kinetic study on the mechanism of hAChE inhibition by hybrid **5**. (A) Overlaid Lineweaver-Burk reciprocal plots of hAChE initial velocity at increasing substrate concentration (ATCh, 0.2–1.6 mM) in the absence of inhibitor and in the presence of **5** (0–10 μM) are shown. Lines were derived from a least-squares analysis of the data points. (B) Replot of slopes vs. inhibitor concentration for calculating K_i as the intersection in the x-axis.

disorders, such as selegiline (IC_{50}=68.7 µM) and moclobemide (IC_{50}=161.4 µM)[85].

The 4-chromenone derivatives **1** (R = 6-OMe) and **4** (R = 5,7-diOH) showed a preference of at least 4.4-times for hMAO-A compared to hMAO-B, whereas the 5-methoxy-4-quinolone hybrid **7** was 6.6-fold more active in hMAO-B than in hMAO-A. Otherwise, the 4-chromenone derivatives **2** (R = 6-OH) and **5** (R = 6,7-diOCH₃) exhibited a balanced inhibitory activity towards hMAO-A and hMAO-B, with IC_{50}s in the low-micromolar range, between 7.0 and 9.7 µM. Interestingly, these values are very close to the IC_{50}s displayed by the well-known antidepressant iproniazid[86] (Table 1).

Furthermore, the antioxidant activities of new hybrids were measured using the oxygen radical absorbance capacity assay (ORAC). Trolox, the aromatic part of vitamin E responsible for its scavenging properties, was used as internal standard with the arbitrary value of ORAC = 1.0. Results are expressed as trolox equivalents (mmol of trolox/mmol of tested compound) in a comparative scale that indicates if a compound is a better (ORAC > 1.0) or a worse scavenger (ORAC < 1.0) than vitamin E. In this assay, only hybrids bearing hydroxyl groups were tested, because we reasonably expected that methoxy-derivatives would not exhibit substantial radical capture capacities according to our previous experience in flavonoid derivatives[32,52]. Thus, all assayed hydroxyl hybrids displayed interesting ORAC values, ranging from 0.5 to 1.6-fold the trolox value. Best results were found in 6-hydroxy derivatives (**2** and **9**, ORAC = 1.6 and 1.2, respectively) and in the 5,7-dihydroxy-4-chromenone hybrid **4** (ORAC = 1.2). The ORAC value clearly dropped for the 4-quinolinone – based hybrid **12** with two adjacent hydroxyl groups in positions 6 and 7 (ORAC = 0.5).

Kinetic analysis of hAChE inhibition

The most potent hAChE inhibitor **5** (IC_{50}=0.99 µM) was selected for studying inhibition kinetics using the Lineweaver-Burk method. The initial velocity of enzymatic inhibition was measured at four concentrations of the substrate acetylthiocholine (ATCh, 0.2–1.6 mM), in absence and presence of increasing concentrations of inhibitor **5** (0.5–10 µM). For each inhibitor concentration,

plotting reciprocals of velocity vs. ATCh concentration (1/V vs. 1/[ATCh]) gave straight lines that were fitted by least-squares analysis (Figure 3). As inhibitor concentration increased, both $1/V_{max}$ (y intercept) and $-1/K_m$ (x intercept) also increased, meaning a mixture of competitive and non-competitive mechanisms in the enzymatic inhibition. This mixed pattern could be due to the simultaneous interaction of hybrid **5** with both CAS and peripheral anionic site (PAS) of hAChE. Replot of slopes vs. inhibitor concentration gave a straight line that was also fitted by least-squares analysis and whose intersection on the negative x-axis provided an estimated inhibition constant (K_i) of 0.95 µM.

Prediction of the CNS-permeation

To check if new compounds could be able to reach their CNS-targets, we used the in vitro parallel artificial membrane permeability assay for the blood-brain barrier (PAMPA-BBB) described by Di et al.[87], and partially modified by us for testing molecules with limited water-solubility[36,46,51–53]. The passive CNS-permeation of new compounds **1–13** through a lipid extract of porcine brain was measured at room temperature. In each experiment, 11 commercial drugs of known brain permeability were also tested and their permeability values normalised to the reported PAMPA-BBB data. According to the patterns previously established in the bibliography[87], compounds with P_e exceeding 4×10^{-6} cm s^{-1} would be able to cross the blood-brain barrier (cns+), whereas those displaying P_e less than 2×10^{-6} cm s^{-1} would not reach the CNS (cns-). All new 4-chromenone – and 4-quinolone – DBMA hybrids **1–13** showed permeability values above 4×10^{-6} cm s^{-1} in this in vitro BBB model (Table 1) and thus, it is expected they could enter into the CNS for interacting with their biological targets.

Inhibition of human BACE-1

New compounds were evaluated as inhibitors of the human recombinant BACE-1 protein, using the fluorescence resonance energy transfer (FRET) assay[88]. Firstly, all compounds were tested at 10 µM giving inhibition percentages below 35%, with the exception of the 6,7-dimethoxy-4-chromenone hybrid with a meta-substitution in the central benzene ring **6**, which blocked around the 80% of the enzymatic activity. Then, the IC_{50} of **6** was calculated from the plot of hBACE-1 activity vs. inhibitor concentrations (0.1–100 µM) giving a value of 6.7 ± 0.8 µM.

Inhibition of human lipoxygenase-5 (hLOX-5)

A selection of new hybrids covering different structural motifs was assayed as inhibitors of hLOX-5, followed the method described by Pufahl et al.[55]. Two well-known inhibitors, namely (R,S)-zileuton and nordihydroguaiaretic acid (NDGA), were used as internal references and results are gathered in Table 2. Tested compounds

Table 2. Inhibition of human hLOX-5 (IC_{50}, µM)[a].

Compd.	X	R	Substitution	IC_{50} (µM)
1	O	6-OMe	4′	12.4 ± 0.5
2	O	6-OH	4′	>100 (38%)
5	O	6,7-diOMe	4′	72.4 ± 2.2
6	O	6,7-diOMe	3′	30.4 ± 1.6
8	NH	6-OMe	4′	>100
10	NH	7-OMe	4′	82.8 ± 4.1
13	NH	6,7-diOMe	3′	36.6 ± 3.1
(R,S)-Zileuton				0.15 ± 0.03
NDGA				0.097 ± 0.019

[a]Results are the mean ± SEM from three independent experiments.

Table 3. Affinity and selectivity towards σ_1 and σ_2 receptors.

Compd.	X	R	Substitution	K_i (µM)[a]		Selectivity vs. $\sigma_1 R$[b]
				$\sigma_1 R$	$\sigma_2 R$	
1	O	6-OMe	4′	0.48 ± 0.05	1.78 ± 0.43	3.7
2	O	6-OH	4′	0.38 ± 0.05	1.60 ± 0.28	4.2
4	O	5,7-diOH	4′	0.51 ± 0.07	> 3.0	> 5.9
6	O	6,7-diOMe	3′	0.53 ± 0.07	1.30 ± 0.35	2.5
Pentazocine				0.015 ± 0.003	n.d.	
DTG				n.d.	0.054 ± 0.008	

[a]Results are expressed as K_i (µM) and are the mean ± SEM of the experiments repeated in triplicates. [b]Selectivity vs. $\sigma_1 R$ was calculated as $K_i \sigma_2 R/K_i \sigma_1 R$. DTG: 1,3-di-o-tolylguanidine.

were modest hLOX-5 inhibitors, the majority of them with IC_{50} values in the two-digit micromolar range.

The best hLOX-5 inhibitor was the 6-methoxy-4-oxochromene hybrid **1** displaying an IC_{50} of 12.4 μM. Interestingly, minimal structural modifications, namely replacement of the methoxy by a hydroxyl group (**2**) or the change of the 4-oxo-chromene by a 4-oxoquinoline ring (**8**), led to inactive compounds.

Studies on sigma receptors

A selection of the most active hybrids in the previous experiments, covering also different structural features, was assayed on sigma receptors using competition experiments with radioligands[56]. Mammalian σ_1 and σ_2 receptors were obtained from guinea pig brain and rat liver, respectively. (+)-Pentazocine (a σ_1-selective ligand) and 1,3-di-o-tolylguanidine (DTG, a σ_2-selective
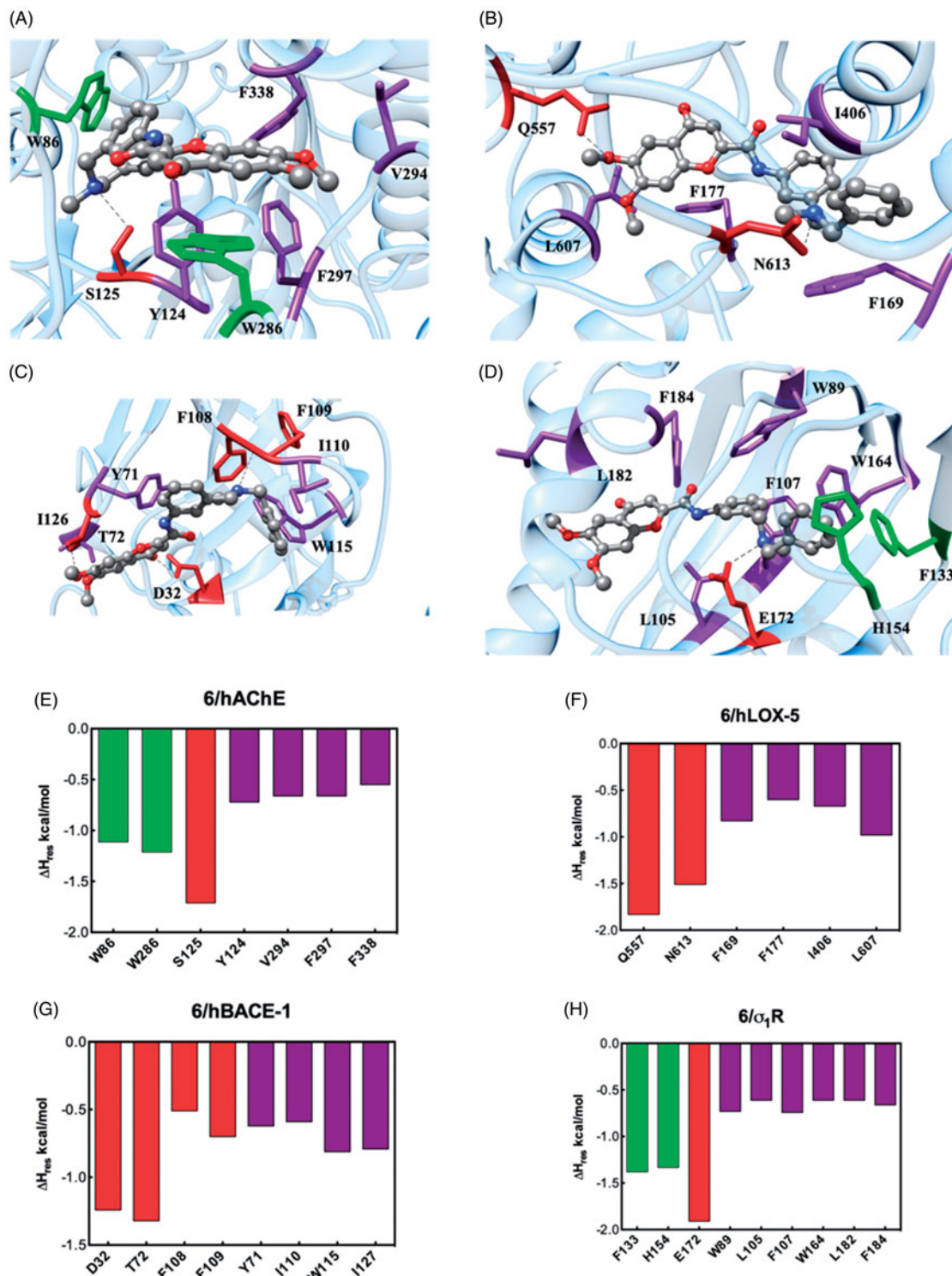

Figure 4. Upper panel: Details of compound **6** in the binding pocket of the hAChE (A), hLOX-5 (B), hBACE-1 (C), and σ_1R (D). Compound **6** is shown as atom-coloured sticks-and-balls (C, grey, N, blue, O, red) while the side chains of proteins residues mainly interacting with **6** are depicted as coloured sticks and labelled. Hydrogen bonds are shown as black broken lines. Hydrogen atoms, water molecules, ions, and counterions are omitted for clarity. Lower panel: Per-residue binding free energy decomposition of the main involved amino acids of the complex between **6** with hAChE (E), hLOX-5 (F), hBACE-1 (G) and σ_1R (H).

ligand) were also evaluated for comparative purposes. Independently from the position of substituents on the 4-oxo-chromene ring and from the relative *meta*- or *para*-substitution of central benzene, all tested hybrids showed selectivity for the σ_1 subtype with K_is in the sub-micromolar range, whereas K_is for the σ_2R displayed one-digit micromolar values (Table 3).

Study of the theoretical medicinal chemistry alerts

In order to choose the best candidate for neurogenic studies, we studied the medicinal chemistry alerts of new flavonoid – DBMA hybrids **1–13** in two free databases, namely ZINC15 (http://zinc15.docking.org/)[73] and SwissADME (http://www.swissadme.ch/)[74]. According to the ZINC15 web site, none of the hybrids was highlighted as pan assay interference compound (PAINS) or aggregator (see Table S1 in Supplementary Information). However, in the SwissADME platform hybrid **12** was marked with a structural alert (catechol), according to the Brenk method[89].

Molecular modelling rationale for the binding of compound 6 against its target proteins

Since 6,7-dimethoxychromone – DBMA **6** resulted to be the new derivative with the most interesting MTD-profile, we carried out molecular dynamics (MD) simulations in order to describe the different binding mechanisms against its biological targets. Accordingly, a putative binding site for **6** was identified on hAChE, hLOX-5, hBACE-1 and σ_1R (Figure 4(A–D)), by applying a well-validated docking protocol[66–68]. Accordingly, MD simulations of the resulting **6**/protein complexes were carried out, and the corresponding ligand/protein free energy of binding (ΔG_{bind}) were calculated via the MM/PBSA (Molecular Mechanics/Poisson-Boltzmann Surface Area) approach[70], yielding values in agreement with relevant experimental activity or affinity.

Afterwards, through a per-residue binding free energy deconvolution (PRBFED) of the enthalpic terms (ΔH_{res}), we were able to

define and describe the different binding mechanisms of **6** to its target proteins (Figure 4(E–H)). The quantification of the single contribution of the main protein residues involved in ligand binding allowed us to rationalise the specific interaction within the different receptor cavities.

Starting from the esterase enzyme, the binding mode of **6** (Figure 4(A)) is fostered by a stable hydrogen bond between the *N*-methyl nitrogen atom with the hydroxyl group of the hAChE S125 side chain ($\Delta H_{res}= -1.71$ kcal/mol, Figure 4(E)). Furthermore, the *N*-benzyl ring is involved in a π-π interaction with W286 ($\Delta H_{res}= -1.21$ kcal/mol), while the flavonoid core of **6** stacks through the chromene moiety against the side chain of W86 ($\Delta H_{res}= -1.11$ kcal/mol). Finally, the **6**/hAChE complex is further stabilised in the putative binding site through hydrophobic interactions between the ligand and the side chains of Y124, V294, F297, and F338 ($\sum\Delta H_{res}= -2.59$ kcal/mol, Figure 4(E)). The sum of these stabilising energies results in favorable ΔG_{bind} values of -7.63 ± 0.23 kcal/mol.

The binding free energy calculated for the **6**/hLOX-5 complex was slightly less favourable than that for hAChE, with a $\Delta G_{bind}= -6.21 \pm 0.25$ kcal/mol. The docking pose of **6** (Figure 4(B)) within the hLOX-5 binding site reveals two stable hydrogen bonds between the DBMA derivative and the lipoxygenase: the basic nitrogen atom acts as acceptor and finds its donor counterpart in the amidic -NH of the side chain of N613 ($\Delta H_{res}= -1.50$ kcal/mol), while a methoxy group of **6** performs a hydrogen bridge with Q557 ($\Delta H_{res}= -1.83$ kcal/mol). Moreover, the aromatic and hydrophobic portions of **6** are nestled in a cavity surrounded by the hLOX-5 residues F169, F177, I406, and L607 ($\sum\Delta H_{res}= -3.08$ kcal/mol, Figure 4(F)).

Molecular modelling procedure was further expanded to analyse the interaction between **6** and human hBACE-1. The favourable binding process thermodynamics reflects into a negative ΔG_{bind} of -7.21 ± 0.28 kcal/mol, supporting the good inhibitory activity of **6** against hBACE-1. In details, the chromene moiety of **6** is involved in two hydrogen bonds with the secretase enzyme
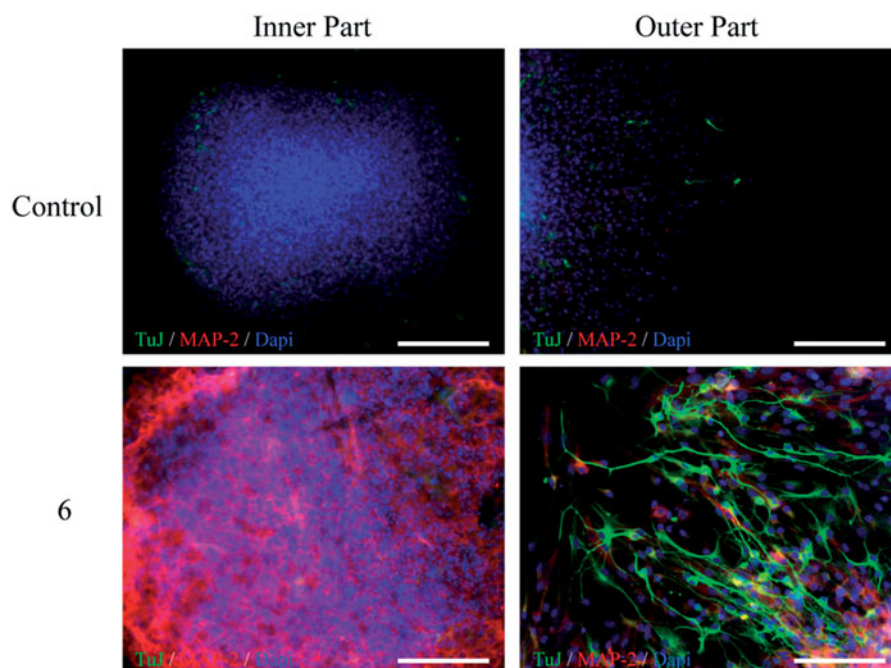

Figure 5. *In vitro* neurogenic effects of chromone-based hybrid **6** (10 μM) on adult mice SGZ-derived NSCs. In the presence of compound **6**, NS were grown for 7 days and allowed to differentiate for 3 additional days. Immunocytochemical analysis shows the expression of two neuronal markers: TuJ1 clone (green) and MAP-2 (red), in the inner and outer part of the NS. DAPI was used for nuclear staining. Scale bar: 20 μm.

(Figure 4(C)): the methoxy substituent interacts with the hydroxyl group of T72 (ΔH_{res}= −1.32 kcal/mol, Figure 4(G)), whilst the acceptor carbonylic group engages its donor counterpart of D32 (ΔH_{res}= −1.24 kcal/mol). A further hydrogen bond is detected between the N-CH$_3$ group of **6** and the backbone amide oxygen atom between F108 and F109 ($\sum\Delta H_{res}$= −1.21 kcal/mol). Additionally, unspecific and favourable contacts are been detected between the lipophilic scaffold of **6** and the secretase residues Y71, I110, W115, and I127 leaning the enzyme binding cavity ($\sum\Delta H_{res}$= −2.81 kcal/mol).

We concluded our computational analysis with the description of the binding mode of **6** onto σ_1R (Figure 4(D)). The interaction spectrum resulting from the analysis of the corresponding MD trajectory (Figure 4(H)) reveals a prototypical pattern of ligand-based intermolecular interactions in the σ_1R cavity: (i) a π-π interaction between the N-benzyl ring with the aromatic side chain of F133 (ΔH_{res}= −1.38 kcal/mol) and H154 (ΔH_{res}= −1.33 kcal/mol); (ii) a permanent salt bridge between the basic N-methyl nitrogen atom

of **6** and the COO$^-$ group of E172 (ΔH_{res}= −1.91 kcal/mol), and (iii) a favourable network of hydrophobic interactions provided by a good insertion of the DBMA derivatives into the σ_1R lipophilic cavity surrounded by the side chains of residues W89, L105, F107, W164, L182, and F184 ($\sum\Delta H_{res}$= −3.95 kcal/mol, Figure 4(H)). This efficient intermolecular interaction scheme is reflected in the good affinity of **6** toward σ_1R, as testified by the favourable value of the free energy of binding ΔG_{bind}= −8.08 ± 0.23 kcal/mol.

Neurogenic studies

Compound **6** with an interesting MTD-profile in hAChE, hLOX-5, hBACE-1 and σ_1R [IC$_{50}$ (hAChE)=4.5 µM; IC$_{50}$ (hLOX-5)=30 µM; IC$_{50}$ (hBACE-1)=6.7 µM; and IC$_{50}$ (σ_1R)=0.53 µM], and without any medicinal chemistry alert, was selected for neurogenic experiments. Thus, we studied the capacity of the chromone-based hybrid **6** to promote neurogenic effects in a primary culture of neural stem-

Table 4. The high scored metabolites of hybrid **6** with reasoning levels of "plausible" and "probable" predictions. Biotransformation names, phase-I enzymes and toxicological effects predictions by Derek v3.2.0. Mutagenic risks assessment by two complementary QSAR methodologies (Derek v3.2.0 and Sarah v3.0.0).

		Derek v3.2.0			Sarah v3.0.0
Compd.	Structure	Bio-transformation name (phase-I enzyme)	Toxicological outcomes	Mutagenic risks	Mutagenic risks
M3		*p*-Hydroxylation of monosubstituted benzene compounds (CYP450)	HERG channel inhibition *in vitro* Plausible	Inactive	Equivocal
M9		Oxidative *O*-demethylation (CYP450)	HERG channel inhibition *in vitro* Plausible	Inactive	Equivocal
M10		Oxidative *O*-demethylation (CYP450)	HERG channel inhibition *in vitro* Plausible	Inactive	Equivocal
M19		Oxidative *O*-demethylation (CYP450)	HERG channel inhibition *in vitro* Plausible	Inactive	Negative 22%
M20		Oxidative *N*-dealkylation (CYP450)	No alerts fired	Inactive	Equivocal
M21		Oxidative *N*-dealkylation (CYP450)	No alerts fired	Inactive	Negative 47%
M22		Oxidative *N*-dealkylation (CYP450)	No alerts fired	Inactive	Equivocal
M23		Oxidative *N*-dealkylation (CYP450)	No alerts fired	Inactive	Negative 100%
M24		Oxidative *N*-dealkylation (CYP450)	No alerts fired	Inactive	Equivocal
M25		Oxidative *N*-dealkylation (CYP450)	No alerts fired	Inactive	Negative 100%

cells (NSCs), isolated from the subgranular zone (SGZ) of adult rats and grown as free-floating neurospheres (NS). Compound was added to NS cultures for 7 days and then, NS were fixed to a substrate and allowed to differentiate in the presence of **6** for a 3-days additional period. Then, we evaluated the expression of β-III-tubulin (TuJ-1 clone; green) and microtubule-associated protein 2 (MAP-2, red) antibodies to visualise early and late neuronal maturation, respectively. As shown in Figure 5, control (basal) experiments (vehicle-treated cultures) only showed a few positive cells for TuJ-1 or MAP-2, whereas in cultures treated with compound **6** the number of both TuJ-1 and MAP-2 marked cells was clearly increased. These results indicate that chromone-based hybrid **6** is able to induce the differentiation of NSCs to a neuronal phenotype *in vitro*.

In silico toxicity and metabolism of hybrid 6

With the aim of advancing one step further in the study of the potential therapeutic success of hybrid **6**, we performed an *in silico* prediction of its toxicity and metabolism, using the Derek Nexus system[78]. The toxicity predictions obtained with Derek Nexus are based on the comparison of the structural features of a given compound with one or more toxicophore patterns (structural alerts) in human species using the Lhasa's knowledge database. Among the 57 toxicity endpoints analysed for hybrid **6**, for 56 of them no alerts were predicted at the minimum reasoning level of "impossible" (See Chart S1 in the Supplementary Information). Only *in vitro* inhibition of the human ether-a-go-go-related gene (hERG) potassium channel was considered "plausible", although with a low-confidence under 67% according to Judson et al.[79]

To add value to the toxicological assessment of hybrid **6**, we performed an *in silico* prediction of its phase-I metabolism in humans, obtaining 10 matching metabolites (Table 4). Potential toxicity was also evaluated for these metabolites with Derek Nexus, in which the minimum likelihood to consider a toxic result in the analysis was "plausible". Results showed that six metabolites were not associated with any structural alerts for toxicity by Derek, and four (M3, M9, M10 and M19) were associated to a "plausible" hERG channel inhibition *in vitro*, also with a confidence under 67%.

Furthermore, each predicted metabolite was selected to evaluate its toxicity and mutagenic potential under the ICH M7 guideline[81] and results are also gathered in Table 4. The carcinogenic risk assessment was carried out with two complementary QSAR methodologies, Derek (KB 2018 1.1) and Sarah (Model 2.0), which predicted an absence of structural alerts for four of the ten metabolites of the hybrid **6**. According to the ICH M7 guide, these results are sufficient to conclude that there is no mutagenic concern and no further tests are recommended for them (Class 5). However, six metabolites obtained an uncertain result, since Derek Nexus predicted a confident negative prediction, while Sarah gave an equivocal prediction. Nevertheless, the equivocal predictions by Sarah are not enough strong to overturn the negative result obtained by Derek. Whereas they are all based on negative results, they have low percentages of confidence, and the confidence level was settled below the 8% as equivocal.

For the parent compound hybrid **6**, in spite of hERG channel inhibition *in vitro*, no other toxicity alerts were fired. Four of the predicted metabolites also showed the same alert. This alert describes a structure-based pharmacophore developed primarily from compounds that have been reported to be inhibitors of the hERG potassium channel[90–92]. The blockage of this channel can lead to the lengthening of the ventricular repolarization phase in the heart, and is characterised on the electrocardiogram as a prolongation of the QT interval[93]. As this is a common feature that makes molecules fall in the preclinical phases, a more deeper investigation should be performed for hybrid **6** and its four metabolites prior to pass to advanced pharmacological assays.

Conclusions

Thirteen new 4-chromenone – DBMA and 4-quinolone – DBMA hybrids were obtained by connecting flavonoid-related structures and an AP2238 fragment. In general, these MTDLs displayed selective inhibition of hAChE (IC$_{50}$s = 0.99–4.5 μM) compared with hBuChE (IC$_{50}$s $> 10 \mu$M) and were CNS-permeable according to the *in vitro* PAMPA-BBB assay. Some hybrids showed micromolar inhibition of hMAO-A (IC$_{50}$s = 1.6–22.8 μM) and hMAO-B (IC$_{50}$s = 8.1–59.8 μM), in many cases with IC$_{50}$ values very close or better than the well-known antidepressants selegiline, iproniazid and moclobemide, concomitantly used in the treatment of AD and PD. Compounds bearing any hydroxyl group in the flavonoid core are good radical scavengers, in some cases 1.6- and 1.2-fold better than vitamin E. Flavonoid – DBMA hybrids were not able to inhibit hBACE-1, with the exception of compound **6** that showed an IC$_{50}$ value of 6.7 μM. Several hybrids were determined to be micromolar inhibitors of hLOX-5, 4-chromenone derivatives being better than their 4-quinolone counterparts. Regarding sigma receptors, all tested hybrids showed affinity values in the micromolar and sub-micromolar scales, with a selectivity of at least 2.5-times in favour to the σ_1R subtype (K_i=0.4–0.5 μM) compared to the σ_2R.

N-(3-((Benzyl(methyl)amino)methyl)phenyl)-6,7-dimethoxy-4-oxo-4*H*-chromene-2-carboxamide (**6**), with an interesting MTD-profile in hAChE, hLOX-5, hBACE-1 and σ_1R [IC$_{50}$ (hAChE)=4.5 μM; IC$_{50}$ (hLOX-5)=30 μM; IC$_{50}$ (hBACE-1)=6.7 μM; and IC$_{50}$ (σ_1R) = 0.5 μM], was selected for a phenotypic assay to study its capacity to promote neurogenic effects. In a primary culture of neural stem-cells from the SGZ of adult rats, hybrid **6** stimulated the differentiation of neural stem-cells to a neuronal phenotype and thus, this hybrid could be a therapeutic agent promoting brain auto-repair processes and blocking early steps of neurodegenerative cascades.

Molecular dynamics simulations of hybrid **6** in hAChE, hLOX-5, hBACE-1 and σ_1R have shown the main interactions with these proteins, providing a rational about the experimental values obtained.

The toxicological alerts for hybrid **6** and its predicted metabolites were promising and relative safe profiles were expected. Nevertheless, the hERG channel inhibition *in vitro* alert was showed, although with a low-confidence below 67%. In next works, *in vivo* studies of hybrid **6** will be carried out to verify its therapeutic actions, its potential cardiac effects, as well as its toxicological behaviour.

Disclosure statement

No potential conflict of interest was reported by the authors.

Supplementary information

Supplementary information includes ^{1}H-NMR, ^{13}C-NMR and HRMS data of flavonoid – DBMA hybrids, and *in silico* predictions of their toxicity and metabolism.

Funding

ORCID

Martín Estrada-Valencia 🔴 http://orcid.org/0000-0001-6350-9785
Clara Herrera-Arozamena 🔴 http://orcid.org/0000-0002-5894-128X
Concepción Pérez 🔴 http://orcid.org/0000-0001-7183-4035
Dolores Viña 🔴 http://orcid.org/0000-0001-5777-1955
José A. Morales-García 🔴 http://orcid.org/0000-0001-9008-0056
Ana Pérez-Castillo 🔴 http://orcid.org/0000-0002-2632-5853
Eva Ramos 🔴 http://orcid.org/0000-0001-5791-0687
Alejandro Romero 🔴 http://orcid.org/0000-0001-5483-4973
Erik Laurini 🔴 http://orcid.org/0000-0001-6092-6532
Sabrina Pricl 🔴 http://orcid.org/0000-0001-8380-4474
María Isabel Rodríguez-Franco 🔴 http://orcid.org/0000-0002-6500-792X

References

1. Scheltens P, Blennow K, Breteler MMB, et al. Alzheimer's disease. Lancet 2016;388:505–17.
2. Zemek F, Drtinova L, Nepovimova E, et al. Outcomes of Alzheimer's disease therapy with acetylcholinesterase inhibitors and memantine. Expert Opin Drug Saf 2014;13:759–74.
3. Wang J, Gu BJ, Masters CL, et al. A systemic view of Alzheimer disease — insights from amyloid-β metabolism beyond the brain. Nat Rev Neurol 2017;13:612.
4. Morphy R, Rankovic Z. Designed multiple ligands. An emerging drug discovery paradigm. J Med Chem 2005;48:6523–43.
5. Bansal Y, Silakari O. Multifunctional compounds: smart molecules for multifactorial diseases. Eur J Med Chem 2014;76:31–42.
6. Ramsay RR, Popovic-Nikolic MR, Nikolic K, et al. A perspective on multi-target drug discovery and design for complex diseases. Clin Transl Med 2018;7:3.
7. Swerdlow RH. Alzheimer's disease pathologic cascades: who comes first, what drives what. Neurotox Res 2012;22:182–94.
8. Hroudova J, Singh N, Fisar Z, et al. Progress in drug development for Alzheimer's disease: an overview in relation to mitochondrial energy metabolism. Eur J Med Chem 2016;121:774–84.
9. Zabel M, Nackenoff A, Kirsch WM, et al. Markers of oxidative damage to lipids, nucleic acids and proteins and antioxidant
10. Moneim AE. Oxidant/antioxidant imbalance and the risk of Alzheimer's disease. Curr Alzheimer Res 2015;12:335–49.
11. Cai Z. Monoamine oxidase inhibitors: promising therapeutic agents for Alzheimer's disease (Review). Mol Med Rep 2014;9:1533–41.
12. Schedin-Weiss S, Inoue M, Hromadkova L, et al. Monoamine oxidase B is elevated in Alzheimer disease neurons, is associated with gamma-secretase and regulates neuronal amyloid beta-peptide levels. Alzheimers Res Ther 2017;9:57.
13. Knez D, Sova M, Kosak U, et al. Dual inhibitors of cholinesterases and monoamine oxidases for Alzheimer's disease. Future Med Chem 2017;9:811–32.
14. MacLeod R, Hillert E-K, Cameron RT, et al. The role and therapeutic targeting of α-, β- and γ-secretase in Alzheimer's disease. Future Sci 2015;1:FSO11.
15. Vassar R, Kandalepas PC. The β-secretase enzyme BACE1 as a therapeutic target for Alzheimer's disease . Alzheimers Res Ther 2011;3:20.
16. May PC, Dean RA, Lowe SL, et al. Robust central reduction of amyloid-β in humans with an orally available, non-peptidic β-secretase inhibitor . J Neurosci 2011;31:16507–16.
17. Evin G, Lessene G, Wilkins S. BACE inhibitors as potential drugs for the treatment of Alzheimer's disease: focus on bioactivity. Recent Pat CNS Drug Discov 2011;6:91–106.
18. Egan MF, Kost J, Tariot PN, et al. Randomized trial of verubecestat for mild-to-moderate Alzheimer's disease. N Engl J Med 2018;378:1691–703.
19. Mullard A. BACE failures lower AD expectations, again. Nat Rev Drug Discov 2018;17:385.
20. Panek D, Więckowska A, Wichur T, et al. Design, synthesis and biological evaluation of new phthalimide and saccharin derivatives with alicyclic amines targeting cholinesterases, beta-secretase and amyloid beta aggregation. Eur J Med Chem 2017;125:676–95.
21. Ikonomovic MD, Abrahamson EE, Uz T, et al. Increased 5-lipoxygenase immunoreactivity in the hippocampus of patients with Alzheimer's disease. J Histochem Cytochem 2008;56:1065–73.
22. Chu J, Giannopoulos PF, Ceballos-Díaz C, et al. 5-Lipoxygenase gene transfer worsens memory, amyloid, and tau brain pathologies in a mouse model of Alzheimer disease. Ann Neurol 2012;72:442–54.
23. Chu J, Li JG, Pratico D. Zileuton improves memory deficits, amyloid and tau pathology in a mouse model of Alzheimer's disease with plaques and tangles. PLoS One 2013;8:e70991.
24. Maurice T, Strehaiano M, Duhr F, et al. Amyloid toxicity is enhanced after pharmacological or genetic invalidation of the σ1 receptor. Behav Brain Res 2018;339:1–10.
25. Qin J, Wang P, Li Y, et al. Activation of sigma-1 receptor by cutamesine attenuates neuronal apoptosis by inhibiting endoplasmic reticulum stress and mitochondrial dysfunction in a rat model of asphyxia cardiac arrest. Shock 2019;51:105–13.
26. Boldrini M, Fulmore CA, Tartt AN, et al. Human hippocampal neurogenesis persists throughout aging. Cell Stem Cell 2018;22:589–99 e585.
27. Sorrells SF, Paredes MF, Cebrian-Silla A, et al. Human hippocampal neurogenesis drops sharply in children to undetectable levels in adults. Nature 2018;555:377–81.

28. Ruscher K, Wieloch T. The involvement of the sigma-1 receptor in neurodegeneration and neurorestoration. J Pharmacol Sci 2015;127:30–5.

29. Herrera-Arozamena C, Martí-Marí O, Estrada M, et al. Recent advances in neurogenic small molecules as innovative treatments for neurodegenerative diseases. Molecules 2016;21: 1165–85.

30. Wang JM, Singh C, Liu L, et al. Allopregnanolone reverses neurogenic and cognitive deficits in mouse model of Alzheimer's disease. Proc Natl Acad Sci USA 2010;107: 6498–503.

31. US National Library of Medicine. Clinical trials.gov (https://clinicaltrials.gov/ct2/show/study/NCT02221622) [last accessed 8 Oct 2018].

32. Estrada Valencia M, Herrera-Arozamena C, de Andrés L, et al. Neurogenic and neuroprotective donepezil-flavonoid hybrids with sigma-1 affinity and inhibition of key enzymes in Alzheimer's disease. Eur J Med Chem 2018;156:534–53.

33. Figueiró-Silva J, Antequera D, Pascual C, et al. The melatonin analog IQM316 may induce adult hippocampal neurogenesis and preserve recognition memories in mice. Cell Transplant 2018;27:423–37.

34. Monjas L, Arce MP, León R, et al. Enzymatic and solid-phase synthesis of new donepezil-based L- and D-glutamic acid derivatives and their pharmacological evaluation in models related to Alzheimer's disease and cerebral ischemia. Eur J Med Chem 2017;130:60–72.

35. Morales-García JA, de la Fuente Revenga M, Alonso-Gil S, et al. The alkaloids of Banisteriopsis caapi, the plant source of the Amazonian hallucinogen ayahuasca, stimulate adult neurogenesis in vitro. Sci Rep 2017;7:5309.

36. de la Fuente Revenga M, Fernández-Sáez N, Herrera-Arozamena C, et al. Novel N-acetyl bioisosteres of melatonin: melatonergic receptor pharmacology, physicochemical studies, and phenotypic assessment of their neurogenic potential. J Med Chem 2015;58:4998–5014.

37. de la Fuente Revenga M, Pérez C, Morales-García JA, et al. Neurogenic potential assessment and pharmacological characterization of 6-methoxy-1,2,3,4-tetrahydro-beta-carboline (pinoline) and melatonin-pinoline hybrids. ACS Chem Neurosci 2015;6:800–10.

38. Lee Y, Jeon SJ, Lee HE, et al. Spinosin, a C-glycoside flavonoid, enhances cognitive performance and adult hippocampal neurogenesis in mice. Pharmacol Biochem Behav 2016;145: 9–16.

39. Shimmyo Y, Kihara T, Akaike A, et al. Flavonols and flavones as BACE-1 inhibitors: structure-activity relationship in cell-free, cell-based and in silico studies reveal novel pharmacophore features. Biochim Biophys Acta 2008;1780:819–25.

40. Ribeiro D, Freitas M, Tome SM, et al. Inhibition of LOX by flavonoids: a structure-activity relationship study. Eur J Med Chem 2014;72:137–45.

41. Carradori S, Gidaro MC, Petzer A, et al. Inhibition of human monoamine oxidase: biological and molecular modeling studies on selected natural flavonoids. J Agric Food Chem 2016;64:9004–11.

42. Tarozzi A, Bartolini M, Piazzi L, et al. From the dual function lead AP2238 to AP2469, a multi-target-directed ligand for the treatment of Alzheimer's disease. Pharmacol Res Perspect 2014;2:e00023.

43. Rizzo S, Bartolini M, Ceccarini L, et al. Targeting Alzheimer's disease: novel indanone hybrids bearing a pharmacophoric fragment of AP2238. Bioorg Med Chem 2010;18:1749–60.

44. Piazzi L, Rampa A, Bisi A, et al. 3-(4-[[Benzyl(methyl)amino]methyl]phenyl)-6,7-dimethoxy-2H-2-chromenone (AP2238) inhibits both acetylcholinesterase and acetylcholinesterase-induced beta-amyloid aggregation: a dual function lead for Alzheimer's disease therapy. J Med Chem 2003;46:2279–82.

45. Wang J, Cai P, Yang XL, et al. Novel cinnamamide-dibenzylamine hybrids: potent neurogenic agents with antioxidant, cholinergic, and neuroprotective properties as innovative drugs for Alzheimer's disease. Eur J Med Chem 2017;139: 68–83.

46. López-Iglesias B, Pérez C, Morales-García JA, et al. New melatonin-N,N-dibenzyl(N-methyl)amine hybrids: potent neurogenic agents with antioxidant, cholinergic, and neuroprotective properties as innovative drugs for Alzheimer's disease. J Med Chem 2014;57:3773–85.

47. Mezeiova E, Spilovska K, Nepovimova E, et al. Profiling donepezil template into multipotent hybrids with antioxidant properties. J Enzyme Inhib Med Chem 2018;33:583–606.

48. Ellman GL, Courtney KD, Andres V, Jr., et al. A new and rapid colorimetric determination of acetylcholinesterase activity. Biochem Pharmacol 1961;7:88–95.

49. Matos MJ, Rodríguez-Enríquez F, Borges F, et al. 3-Amidocoumarins as potential multifunctional agents against neurodegenerative diseases. ChemMedChem 2015;10: 2071–9.

50. Dávalos A, Gómez-Cordovés C, Bartolomé B. Extending applicability of the oxygen radical absorbance capacity (ORAC-fluorescein) assay. J Agric Food Chem 2004;52:48–54.

51. Rodríguez-Franco MI, Fernández-Bachiller MI, Pérez C, et al. Novel tacrine-melatonin hybrids as dual-acting drugs for Alzheimer disease, with improved acetylcholinesterase inhibitory and antioxidant properties. J Med Chem 2006;49: 459–62.

52. Fernández-Bachiller MI, Pérez C, Monjas L, et al. New tacrine–4-oxo-4H-chromene hybrids as multifunctional agents for the treatment of Alzheimer's disease, with cholinergic, antioxidant, and beta-amyloid-reducing properties. J Med Chem 2012;55:1303–17.

53. Reis J, Cagide F, Estrada Valencia M, et al. Multi-target-directed ligands for Alzheimer's disease: discovery of chromone-based monoamine oxidase/cholinesterase inhibitors. Eur J Med Chem 2018;158:781–800.

54. BACE1 (β-secretase) FRET assay kit, part # P2985, Invitrogen (http://tools.invitrogen.com/content/sfs/manuals/L0724.pdf) [last accessed 12 Jun 2018].

55. Pufahl RA, Kasten TP, Hills R, et al. Development of a fluorescence-based enzyme assay of human 5-lipoxygenase. Anal Biochem 2007;364:204–12.

56. Chu UB, Ruoho AE. Sigma receptor binding assays. Curr Protoc Pharmacol 2015;71:1 34 31–21.

57. Case DA, Betz RM, Botello-Smith W, et al. AMBER 18. San Francisco (CA, USA): University of California; 2018.

58. Pettersen EF, Goddard TD, Huang CC, et al. UCSF Chimera-a visualization system for exploratory research and analysis. J Comput Chem 2004;25:1605–12.

59. Cheung J, Rudolph MJ, Burshteyn F, et al. Structures of human acetylcholinesterase in complex with pharmacologically important ligands. J Med Chem 2012;55:10282–6.

60. Gilbert NC, Rui Z, Neau DB, et al. Conversion of human 5-lipoxygenase to a 15-lipoxygenase by a point mutation to mimic phosphorylation at Serine-663. FASEB J 2012;26: 3222–9.

61. Hong L, Turner RT, 3rd, Koelsch G, et al. Crystal structure of memapsin 2 (beta-secretase) in complex with an inhibitor OM00-3. Biochemistry 2002;41:10963–7.

62. Schmidt HR, Zheng S, Gurpinar E, et al. Crystal structure of the human σ1 receptor. Nature 2016;532:527–30.

63. Laurini E, Col VD, Mamolo MG, et al. Homology model and docking-based virtual screening for ligands of the σ1 receptor. ACS Med Chem Lett 2011;2:834–9.

64. Brune S, Schepmann D, Klempnauer KH, et al. The sigma enigma: in vitro/in silico site-directed mutagenesis studies unveil sigma1 receptor ligand binding. Biochemistry 2014; 53:2993–3003.

65. Morris GM, Huey R, Lindstrom W, et al. AutoDock4 and AutoDockTools4: automated docking with selective receptor flexibility. J Comput Chem 2009;30:2785–91.

66. Laurini E, Marson D, Dal Col V, et al. Another brick in the wall. Validation of the sigma1 receptor 3D model by computer-assisted design, synthesis, and activity of new sigma1 ligands. Mol Pharm 2012;9:3107–26.

67. Briguglio I, Loddo R, Laurini E, et al. Synthesis, cytotoxicity and antiviral evaluation of new series of imidazo[4,5-g]quinoline and pyrido[2,3-g]quinoxalinone derivatives. Eur J Med Chem 2015;105:63–79.

68. Estrada M, Pérez C, Soriano E, et al. New neurogenic lipoic-based hybrids as innovative Alzheimer's drugs with sigma-1 agonism and beta-secretase inhibition. Future Med Chem 2016;8:1191–207.

69. Jorgensen WL, Chandrasekhar J, Madura JD, et al. Comparison of simple potential functions for simulating liquid water. J Chem Phys 1983;79:926–35.

70. Massova I, Kollman PA. Combined molecular mechanical and continuum solvent approach (MM-PBSA/GBSA) to predict ligand binding. Perspect Drug Discov 2000;18:113–35.

71. Tsui V, Case DA. Theory and applications of the generalized Born solvation model in macromolecular simulations. Biopolymers 2000;56:275–91.

72. Onufriev A, Bashford D, Case DA. Modification of the generalized Born model suitable for macromolecules. J Phys Chem B 2000;104:3712–20.

73. Sterling T, Irwin JJ. ZINC 15-ligand discovery for everyone. J Chem Inf Model 2015;55:2324–37.

74. Daina A, Michielin O, Zoete V. SwissADME: a free web tool to evaluate pharmacokinetics, drug-likeness and medicinal chemistry friendliness of small molecules. Sci Rep 2017;7: 42717.

75. Morales-García JA, Alonso-Gil S, Gil C, et al. Phosphodiesterase 7 inhibition induces dopaminergic neurogenesis in hemiparkinsonian rats. Stem Cells Transl Med 2015;4:564–75.

76. Morales-García JA, Luna-Medina R, Alfaro-Cervello C, et al. Peroxisome proliferator-activated receptor gamma ligands regulate neural stem cell proliferation and differentiation in vitro and in vivo. Glia 2011;59:293–307.

77. Morales-García JA, Luna-Medina R, Alonso-Gil S, et al. Glycogen synthase kinase 3 inhibition promotes adult hippocampal neurogenesis in vitro and in vivo. ACS Chem Neurosci 2012;3:963–71.

78. Marchant CA, Briggs KA, Long A. In silico tools for sharing data and knowledge on toxicity and metabolism: Derek for windows, meteor, and vitic. Toxicol Mech Methods 2008;18: 177–87.

79. Judson PN, Stalford SA, Vessey J. Assessing confidence in predictions made by knowledge-based systems. Toxicol Res 2013;2:70–9.

80. Al Sharif M, Alov P, Vitcheva V, et al. Natural modulators of nonalcoholic fatty liver disease: mode of action analysis and in silico ADME-Tox prediction. Toxicol Appl Pharmacol 2017; 337:45–66.

81. ICH Harmonised Guideline. Assessment and control of DNA reactive (mutagenic) impurities in pharmaceuticals to limit potential carcinogenic risk. 2017, http://www.ich.org/products/guidelines/multidisciplinary/article/multidisciplinary-guidelines.html.

82. OECD, Guidance document on the validation of (quantitative) structure-activity relationship [(Q)SAR] models. 2014; doi:https://doi.org/10.1787/9789264085442-en.

83. McOmie JFW, Watts ML, West DE. Demethylation of aryl methyl ethers by boron tribromide. Tetrahedron 1968;24: 2289–92.

84. Matos MJ, Rodríguez-Enríquez F, Vilar S, et al. Potent and selective MAO-B inhibitory activity: amino- versus nitro-3-arylcoumarin derivatives. Bioorg Med Chem Lett 2015;25: 642–8.

85. Finberg JP, Rabey JM. Inhibitors of MAO-A and MAO-B in psychiatry and neurology. Front Pharmacol 2016;7:340.

86. Dhir A. Investigational drugs for treating major depressive disorder. Expert Opin Investig Drugs 2017;26:9–24.

87. Di L, Kerns EH, Fan K, et al. High throughput artificial membrane permeability assay for blood-brain barrier. Eur J Med Chem 2003;38:223–32.

88. Mancini F, Naldi M, Cavrini V, et al. Multiwell fluorometric and colorimetric microassays for the evaluation of beta-secretase (BACE-1) inhibitors. Anal Bioanal Chem 2007;388: 1175–83.

89. Brenk R, Schipani A, James D, et al. Lessons learnt from assembling screening libraries for drug discovery for neglected diseases. ChemMedChem 2008;3:435–44.

90. Pearlstein RA, Vaz RJ, Kang J, et al. Characterization of HERG potassium channel inhibition using CoMSiA 3D QSAR and homology modeling approaches. Bioorg Med Chem Lett 2003;13:1829–35.

91. Cavalli A, Poluzzi E, De Ponti F, et al. Toward a pharmacophore for drugs inducing the long QT syndrome: insights from a CoMFA study of HERG K(+) channel blockers. J Med Chem 2002;45:3844–53.

92. Ekins S, Crumb WJ, Sarazan RD, et al. Three-dimensional quantitative structure-activity relationship for inhibition of human ether-a-go-go-related gene potassium channel. J Pharmacol Exp Ther 2002;301:427–34.

93. Crumb W, Cavero II. QT interval prolongation by non-cardiovascular drugs: issues and solutions for novel drug development. Pharm Sci Tech Today 1999;2:270–80.